Margarida Seabra Leiria de Matos Glória

Licenciatura em Engenharia de Micro e Nanotecnologias

Engineering of hybrid composite systems based on nanocellulose and magnetic nanoparticles for biomedical applications

Dissertação para obtenção do Grau de Mestre em

Engenharia de Micro e Nanotecnologias

Orientador: Doutora Paula Isabel Pereira Soares, Investigadora em Pós-doutoramento, CENIMAT/I3N – Departamento de Ciências dos Materiais, Faculdade de Ciências e Tecnologia da Universidade Nova de Lisboa

Co-orientador: Doutora Susete Maria Brazão Nogueira Fernandes, Investigadora, CENIMAT/I3N - Departamento de Ciência dos Materiais, Faculdade de Ciências e Tecnologia da Universidade Nova de Lisboa

Presidente: Doutor Hugo Manuel Brito Águas, Professor Associado, FCT-UNL

Arguente: Doutor João Paulo Miranda Ribeiro Borges, Professor Associado com Agregação, FCT-UNL

Vogal: Doutora Paula Isabel Pereira Soares, Investigadora em Pós-doutoramento, FCT-UNL

FACULDADE DE CIÊNCIAS E TECNOLOGIA
UNIVERSIDADE NOVA DE LISBOA

Dezembro, 2019

Engineering of hybrid composite systems based on nanocellulose and magnetic nanoparticles for biomedical applications

“If you are going through hell, keep going”

Winston Churchill

Acknowledgements

Em primeiro lugar devo agradecer à Faculdade de Ciências e Tecnologia, a instituição que me acolheu com tão bom ambiente e ao Departamento de Ciências dos Materiais e Cenimat, onde pude aprender tanto e desenvolver o meu trabalho.

Quero agradecer à minha orientadora, Doutora Paula Soares, por me ter aceite nesta tese, e por toda a *guidance* ao longo destes meses. Foi um prazer ter sido aceite num tema que tinha como orientadora a oradora de uma certa aula de bionanotecnologia que me deixou boquiaberta. Para além da óbvia orientação e correções muito necessárias, as palavras encorajadoras vieram nos momentos mais críticos e ajudaram bastante.

À minha co-orientadora, Doutora Susete Fernandes, tenho de agradecer pelo interesse que fomentou nas aulas de Materiais Celulósicos e Papel, que eventualmente se tornou em interesse acrescido por este tema. A exigência e a atenção ao pormenor foram sempre pertinentes, ainda que os "*Não chore!"* nem sempre tenham sido eficazes.

Ao Ricardo Chagas, rei do desenrascar, que não tarda será beatificado, pela sua infinita paciência para me ajudar e ensinar. As noções químicas perdidas em mim voltaram à superfície! No inferno, estaremos os dois, lado a lado, hora a hora, a arranjar agitadores orbitais com elásticos de escritório.

Gostava de agradecer também à Professora Célia Henriques e Ana Catarina Pinto por toda ajuda prestada no laboratório de cultura celular, ao Professor João Canejo e ao Pedro Silva pelo auxílio.

É importante agradecer ao Doutor Rodrigo Martins e à Doutora Elvira Fortunato, por terem criado este curso tão especial, que tem um papel tão importante para mim. Costumo dizer, se não fosse este curso, não seria mais nenhum. Por estar tão feliz e realizada nele, tive oportunidade de me envolver numa imensidão de eventos e atividades extracurriculares.

Ao Diogo Saraiva, por me ter dado as boas-vindas no laboratório e nunca dizer que não aos meus pedidos e dúvidas (não deixei nenhum cabelo meu nas tuas celuloses!). Dia bom.

À Bibi, somos duas almas gémeas separadas durante uma vida que se juntaram durante a tese. Ao Miguel Carreto, à Adriana, à Bárbara, à Rita, ao Lavadinho, à Sofia: foi um prazer ter momentos de desespero sincronizados.

Ao meu melhor amigo, João, por estar sempre disponível nos piores momentos, pela honestidade, pelas *midnight drives*. Viajarei até ao fim do mundo para encontrar caixas de 20 *nuggets* para ti. No Céu, estaremos a ver *vines* em *loop*.

Ao meu grupo de amigos que esteve lá desde o 1º dia, e em tantas noites de estudo na 202: João Ricardo, Ricardo, Joana, Hadassa, Carolina e JP. Aprendi tanto com vocês todos e não teria sido o mesmo enfrentar todos os desafios sem vocês. *I had the time of my life fighting dragons with you*.

À minha gente que se vestiu de negro comigo, Bernardo, Inês, Neto, Matos, Recife. Aos restantes colegas de curso que não menciono, mas que foram tão boa companhia.

Às pessoas da Associação DOS Estudantes do mandato de 2019, encontrei em vocês uma família. Foi um espaço de imenso crescimento pessoal, onde entendi o verdadeiro significado de equipa. Obrigada por me ensinarem tanto e pelos bons momentos passados, quase que nem sinto o desmontar das festas no frio das 4 da manhã. Agradecimentos em especial à Carolina (mãe!) e ao Pedro, o meu parceiro e *fellow* batata-casada.

Ao grupo de amigos que *somehow* consegui manter com muito esporádico contacto ao longo de 5 anos: Filipa, Nunes, Catarina, Ana, Marcelo, Ivan, Kaos, Tiques (ambos), Inês, Rute, Messias. Obrigada pela oportunidade de falar de faculdade, fora da faculdade.

Ao meu Pai (não fiques vaidoso), por me ter dissimuladamente impedido de ir para artes e ter chamado à atenção para a existência deste magnífico curso. À minha Mamã, pelo inglês desde pequenina, pelos sacos de água quente durante o estudo, pelas boleias tardias, pelo *counseling*, pelo apoio incondicional. Aos manos, pelos *role-models* que foram (e são!) e que sempre acreditaram em mim, mesmo quando eu não o fazia.

Ao Miguel, um pedido de desculpas para além do agradecimento, foram 5 anos difíceis e apoiaste-me sempre. Obrigada por simplificares os meus problemas e me atirares comida quando necessário.

Este trabalho foi financiado utilizando fundos concedidos pela FEDER através do Programa COMPETE 2020 e Fundos Nacionais, através da FCT – Fundação para a Ciência e Tecnologia e também POR Lisboa2020 ao abrigo do projeto POCI – 01-0145-FEDER-007688 (Referência UID/CTM/50025), PTDC/CTM-CTM/30623/2017 e PTDC/CTM-REF/30529/2017 (NanoCell2SEC).

Resumo

Atualmente existe um número crescente de pessoas que sobrevive ao cancro, apesar da incidência e as mortes relacionadas continuarem a aumentar ao longos dos anos. As terapias atuais para o cancro como radioterapia e quimioterapia causam vários efeitos colaterais negativos que afetam significativamente o bem-estar do paciente. Em alternativa, a hipertermia magnética induz um aumento da temperatura em células tumorais devido à aplicação de um campo magnético alternado. Este aumento da temperatura é suficiente para desencadear um número de mecanismos que induzem a morte de células cancerígenas, que são mais sensíveis à temperatura, sem prejudicar células saudáveis.

O objetivo desta tese é produzir um novo biomaterial para a aplicação da hipertermia magnética baseado em dois materiais: as já reportadas nanopartículas superparamagnéticas de Fe_3O_4 (SPIONs) capazes de induzir calor; e nanocristais de celulose (CNCs), um eficiente reforço mecânico amigo do ambiente. Assim, um novo material compósito utilizando álcool polivinílico (PVA) como matriz foi produzido combinando os dois materiais acima referidos. Dois tipos de estruturas foram produzidos dependendo do agente reticulante utilizado: filmes com ácido cítrico e hidrogéis com glutaraldeído. As propriedades físico-químicas, assim como as propriedades estruturais, foram avaliadas por DRX e FTIR. Adicionalmente, a capacidade de inchamento e as propriedades mecânicas foram testadas através de testes de inchamento e de compressão. Finalmente, foram efetuados testes *in vitro* para avaliar a *performance* destes materiais compósitos.

Tanto os filmes como os hidrogéis mostraram resposta quando submetidos a um magneto permanente, absorveram o valor da sua massa em água, e apresentaram propriedades mecânicas promissoras. Os hidrogéis de PVA, PVA/CNC, e PVA/CNC/NP apresentaram um módulo de compressão de 0,76 ± 0,22, 1,45 ± 0,55 e 1,05 ± 0,17 MPa, respetivamente.

Os filmes produziram um aumento de 1.8 °C, enquanto os hidrogéis atingiram 2.1 °C sob aplicação de um campo magnético alternado. Os materiais compósitos são biocompatíveis tendo em conta a composição testada, demonstrando a aplicação promissora destes materiais em condições fisiológicas.

Palavras-chave: hipertermia magnética, SPIONs, CNC, PVA, ácido cítrico, glutaraldeído

Abstract

Nowadays an increasing number of people survive cancer, still the incidence and related deaths continue to increase over the years. Current cancer therapies like radiation and chemotherapy cause several negative side effects that significantly affect the patient's wellbeing. In alternative, magnetic hyperthermia induces a temperature increase in tumor cells due to the application of an alternating magnetic field. This rise in temperature is enough to trigger a set of mechanisms that induce the death of the cancerous cells, which are more sensitive to temperature, without harming healthy cells.

The goal of this thesis was to produce a new biomaterial for magnetic hyperthermia application based on two materials: the well-reported heat-inducer Fe_3O_4 superparamagnetic nanoparticles; and cellulose nanocrystals (CNCs), an effective green mechanical reinforcement. Thus, a new composite material using polyvinyl alcohol (PVA) as a matrix was produced combining the two above-mentioned materials. Two types of structures were produced depending on the crosslinker used: films with citric acid, and hydrogels with glutaraldehyde. The physicochemical properties, as well as structural properties, were evaluated by XRD and FTIR. Additionally, swelling ability and mechanical properties were assessed with water uptake and compression tests. Finally, *in vitro* tests were made to evaluate the performance of these composite materials.

Both films and hydrogels were able to respond to a permanent magnet, absorbed their weight in water, and presented promising mechanical properties. PVA, PVA/CNC, and PVA/CNC/NP hydrogels displayed a compressive modulus of 0.76 ± 0.22, 1.45 ± 0.55 and 1.05 ± 0.17 MPa, respectively.

The films managed to produce a 1.8 °C increase in temperature, while the hydrogels reached 2.1 °C under the application of an external alternating magnetic field. The composite materials are biocompatible within the tested composition, demonstrating the promising application of these materials in physiological conditions.

Keywords: magnetic hyperthermia, SPIONs, CNC, PVA, citric acid, glutaraldehyde

Table of contents

ACKNOWLEDGEMENTS VII

RESUMO IX

ABSTRACT 11

LIST OF FIGURES 15

LIST OF TABLES 19

ACRONYMS 21

1 CONTEXT 1

2 INTRODUCTION 3

2.1 Magnetic Hyperthermia 3

2.2 Superparamagnetic Iron Oxide Nanoparticles 4

2.3 Cellulose Nanocrystals 4

2.4 Polyvinyl Alcohol 5

2.5 Composite's state of the art 7

3 MATERIALS AND METHODS 9

3.1 Synthesis of cellulose nanocrystals 9

3.2 Iron Oxide Nanoparticles Synthesis 9

3.3 Ternary Composite 9

3.4 Water Uptake tests 10

3.5 In vitro tests 10

3.6 Magnetic Hyperthermia 10

3.7 Mechanical Tests 10

3.8 Characterization 10

4 RESULTS AND DISCUSSION 11

4.1 Cellulose nanocrystals' production 11

4.2 Hybrid composite system – preliminary work 16

4.3 Hybrid composite system production 19

4.4 Hybrid composite system characterization 23

5 CONCLUSIONS AND FUTURE PERSPECTIVES 32
6 REFERENCES 35
7 SUPPORTING INFORMATION 41
7.1 Cellulose Nanocrystals 41
7.2 Iron Oxide Nanoparticles' Synthesis 41
7.3 In vitro tests 42
7.4 Characterization Techniques 43
7.5 Mechanical Tests 44

List of figures

FIGURE 2.1 – REPRESENTATION OF NÉEL AND BROWN RELAXATION MECHANISMS. THE BROWN CIRCLES REPRESENT THE SUPERPARAMAGNETIC IRON OXIDE NANOPARTICLES [19]. 3

FIGURE 2.2 - REPRESENTATION OF A) CELLULOSE FIBERS, WHERE THE CRYSTALLINE AND AMORPHOUS REGIONS ARE DEPICTED, B) CELLOBIOSE, THE REPETITIVE DIMER OF THE POLYMER CELLULOSE AND THE EFFECT OF SULFURIC ACID HYDROLYSIS IN THE POLYMER ADAPTED FROM [37]. 5

FIGURE 2.3 -REACTION SCHEME SHOWING BOTH INTERMOLECULAR AND INTRAMOLECULAR CROSSLINKING OF PVA USING CITRIC ACID [46]. 6

FIGURE 2.4 - REACTION BETWEEN PVA (1) AND GA (2) IN ACID CONDITIONS PROVIDED BY HYDROCHLORIC ACID, RESULTING IN CROSSLINKED PVA BY ACETAL BRIDGES (3) WITH THE RELEASE OF WATER [48]. 6

FIGURE 4.1 - DIAGRAM OF H+ TO NA+ PROTON SUBSTITUTION IN CNCS AFTER CONTACT IN NA PROTONATED ION-EXCHANGE RESIN 12

FIGURE 4.2 – ATR-FTIR SPECTROGRAMS OF THE PRECURSOR MATERIAL - MCC, CNC AND SODIUM CNCS (CNC NA). 13

FIGURE 4.3 - XRD DIFFRACTOGRAMS OF THE PRECURSOR MATERIAL - MCC, CNC AND SODIUM TREATED CNCS (CNC NA). 13

FIGURE 4.4 – AFM-ACQUIRED TOPOGRAPHIC IMAGE, IN AMPLITUDE MODE, SHOWING INDIVIDUALIZED CNC, AND THE RESPECTIVE DISTRIBUTION OF MEASUREMENTS REGARDING LENGTH AND WIDTH OF THE NANOCRYSTALS. 14

FIGURE 4.5 – DIFFERENTIAL THERMAL ANALYSIS OF MICROCRYSTALLINE CELLULOSE, CNC, AND SODIUM PROTONATED CNC. A) THE GRAPH FOR THERMOGRAVIMETRIC MEASUREMENTS. B) THE DIFFERENTIAL SCANNING CALORIMETRY ANALYSIS IS PRESENTED. 15

FIGURE 4.6 - PHOTOGRAPHS OF HYBRID CNC AND SPION FILMS PREVIOUSLY PRODUCED BY THE SBMG. A) NO POLARIZER B) LEFT CIRCULAR POLARIZER C) RIGHT CIRCULAR POLARIZER. SAME SCALE APPLIES TO ALL OF THE IMAGES IN THE COMPOSITION. 16

FIGURE 4.7 - FILM MADE FROM SODIUM TREATED CNCS BY FULL SOLVENT EVAPORATION AT 37 °C. PHOTOGRAPHS OF SAID FILM: A) UNPOLARIZED WHITE LIGHT B) LEFT CIRCULAR POLARIZER C) RIGHT CIRCULAR POLARIZER. D), E) AND F) ARE POLARIZED OPTICAL MICROSCOPY IMAGES OF THE SAME FILMS. 17

FIGURE 4.8 –SPIONS CHARACTERIZATION: A) TEM IMAGE OF BARE Fe_3O_4 NPS B) TEM IMAGE OF DMSA-COATED Fe_3O_4 NPS C) XRD SPECTRA OF BOTH BARE AND DMSA-COATED Fe_3O_4 NPS D) HYDRODYNAMIC DIAMETERS OF DMSA-COATED Fe_3O_4 NPS [8] 17

FIGURE 4.9 - ADHESION AND PROLIFERATION OF VERO CELLS ON CNC AND CNC/NP FILMS THROUGHOUT 10 DAYS MEASURED USING THE RESAZURIN METHOD. THE LAST COLUMN, CC, REFERS TO THE CELL CONTROL. 18

FIGURE 4.10 – FLUORESCENCE MICROSCOPY IMAGES FROM MICROSCOPE NIKON ECLIPSE TI-S OF A) CONTROL CELLS, B) CELLS ADHERED TO CNC FILMS AND C) CELLS ADHERED TO CNC/SPIONS FILMS. CELL'S CYTOSKELETON IS VISIBLE IN RED AND THE NUCLEI IN BLUE. 19

FIGURE 4.11 - PHOTOGRAPHS OF PVA FILMS WITH INCREASING CONCENTRATION OF CNC: A) 0 WT.%, B) 0.5 WT.%, C) 1 WT.%, D) 2 WT.% E) 5 WT.%. SAME SCALE APPLIES TO ALL OF THE IMAGES IN THE COMPOSITION. 19

FIGURE 4.12 – A) STUDY OF INCORPORATION OF SPIONS IN PVA FILMS OBTAINED BY SOLVENT EVAPORATION. FROM LEFT TO RIGHT: 0.5 WT.%, 5 WT.% AND 7.5 WT.% SPIONS IN RESPECT TO PVA CONTENT. B) CA-CROSSLINKED FILM AT 130 °C, WITH 10 WT.% SPIONS PRIOR TO WASHING. 20

FIGURE 4.13 - PRE-STUDY OF THE CONCENTRATIONS OF CROSSLINKER TO BE USED. IN THE LEFT PICTURE A), 1 % OF GA+ 0.4 % OF HCL. IN THE RIGHT PICTURE B), 10 % OF GA + 4 % HCL. 21

FIGURE 4.14 – PHOTOGRAPHS DEPICTING THE OBVIOUS DARKENING OF THE CITRIC ACID-CROSSLINKED FILMS CATALYZED WITH HCL AT 130 °C. TOP VIEW OF: A) PVA/CA B) PVA/CNC/CA AND C) PVA/CNC/NP/CA. SAME SCALE APPLIES TO ALL OF THE IMAGES IN THE COMPOSITION. 22

FIGURE 4.15 – PHOTOGRAPHS OF THE TOP VIEW OF THE OPTIMIZED CA-CROSSLINKED FILMS AT 130 °C DURING 5 H IN THE ABSENCE OF CATALYST (AFTER WASHING AND DRYING): A) PVA, B) PVA/CNC AND PVA/CNC/NP. SAME SCALE APPLIES TO ALL OF THE IMAGES IN THE COMPOSITION 22

FIGURE 4.16 – PHOTOGRAPHS OF TOP AND SIDE VIEW OF THE OPTIMIZED GA-CROSSLINKED HYDROGELS AT ROOM TEMPERATURE: A) PVA B) PVA/CNC C) PVA/CNC/NP. 23

FIGURE 4.17 - XRD DIFFRACTOGRAMS FOR PVA, A) CA-CROSSLINKED SAMPLES: PVA, PVA/CNC AND PVA/CNC/NP, AND B) GA-CROSSLINKED SAMPLES: PVA, PVA/CNC AND PVA/CNC/NP. 24

FIGURE 4.18 - FTIR SPECTRA OF A) CITRIC ACID-CROSSLINKED PVA FILMS AND B) GA-CROSSLINKED FILMS: PRISTINE PVA, CROSSLINKED PVA FILM, PVA/CNC CROSSLINKED FILMS, AND PVA/CNC/NP CROSSLINKED FILMS. 25

FIGURE 4.19 – THERMOGRAVIMETRIC ANALYSIS OF NEAT PVA, A) CA-CROSSLINKED AND B) GA-CROSSLINKED SAMPLES: PVA, PVA/CNC, PVA/CNC/NP. 26

FIGURE 4.20 - WATER UPTAKE VALUES FOR A) CA-CROSSLINKED AND B)GA-CROSSLINKED PVA HYDROGELS: SIMPLE PVA/CA FILMS, WITH CNC, AND BOTH CNC AND SPIONS 27

FIGURE 4.21 – ON THE LEFT, TENSILE CURVES FROM NEAT PVA AND CA-CROSSLINKED FILMS. PVA, PVA/CNC AND PVA/CNC/NP ALL DISPLAY TYPICAL BEHAVIORS. ON THE RIGHT, AN EXAMPLE OF THE TENSILE TEST ON THE FILMS. 28

FIGURE 4.22 – EXAMPLE OF COMPRESSION CURVE. IN THIS GRAPH OF A GA-CROSSLINKED PVA HYDROGEL, A STEEP EXPONENTIAL CURVE IS OBSERVED UNTIL FRACTURE. A CLOSE-UP OF THE CURVE BETWEEN 10 AND 20 % DEFORMATION IS PICTURED WITH ITS LINEAR FIT. 29

FIGURE 4.23 - CYTOTOXICITY OF CA CROSSLINKED FILMS: PVA, PVA/CNC AND PVA/CNC/NP WERE ALL TESTED FOR DIFFERENT CONCENTRATIONS (50, 25, 12.5 AND 6.25 MG/ML). THE LAST COLUMN, C-, REFERS TO THE VALUES OF THE NEGATIVE CONTROL..... 30

FIGURE 4.24 - CYTOTOXICITY OF GA CROSSLINKED GELS: PVA, PVA/CNC AND PVA/CNC/NP WERE ALL TESTED FOR DIFFERENT CONCENTRATIONS (50, 25, 12.5 AND 6.25 MG/ML). THE LAST COLUMN, C-, REFERS TO THE VALUES OF THE NEGATIVE CONTROL..... 31

FIGURE 4.25 - TEMPERATURE VARIATION DEPENDING ON THE TYPE OF SAMPLE: CA-CROSSLINKED FILM OR GA-CROSSLINKED HYDROGEL. THE SAME AMOUNT OF SPIONS INCLUDED IN THE SAMPLES WAS TESTED IN SOLUTION FOR COMPARISON SAKE..... 31

FIGURE 7.1 - EXAMPLE OF COMPRESSION CURVE. IN THIS GRAPH OF A GA-CROSSLINKED PVA/CNC HYDROGEL, A STEEP EXPONENTIAL CURVE IS OBSERVED UNTIL FRACTURE..... 44

FIGURE 7.2 - EXAMPLE OF COMPRESSION CURVE. IN THIS GRAPH OF A GA-CROSSLINKED PVA/CNC/NP HYDROGEL, A STEEP EXPONENTIAL CURVE IS OBSERVED UNTIL FRACTURE..... 45

List of tables

TABLE 4.1 – VALUES OF THE ELEMENTS C, N, H AND S DETECTED BY ELEMENTAL ANALYSIS ON THE PRECURSOR, FINAL CNC MATERIAL AND VALUES PREDICTED FOR PURE CELLULOSE. THE VALUES ARE PRESENTED IN PERCENTAGE; THE AMOUNT OF OXYGEN (*) WAS CALCULATED BY DIFFERENCE. 12

TABLE 4.2 –TESTED CONDITIONS TO CROSSLINK THE HYBRID COMPOSITE SYSTEM DEPENDING ON THE CROSSLINKING AGENT, PRESENCE OF CATALYST, REACTION TEMPERATURE, AND THE RESPECTIVE RESULTS..... 21

TABLE 7.1 - DATA OBTAINED FROM THE GA CROSSLINKED PVA HYDROGEL FOR THE COMPRESSIVE TEST RUNS 44

TABLE 7.2 - DATA OBTAINED FROM THE GA CROSSLINKED PVA/CNC HYDROGEL FOR THE COMPRESSIVE TEST RUNS..... 45

TABLE 7.3 - DATA OBTAINED FROM THE GA CROSSLINKED PVA/CNC/NP HYDROGEL FOR THE COMPRESSIVE TEST RUNS 45

Acronyms

AFM	Atomic Force Microscopy
AMF	Alternating Magnetic Field
ATR	Attenuated Total Reflectance
CA	Citric Acid
CNC	Cellulose Nanocrystal
DMSA	Dimercaptosuccinic Acid
DSC	Differential Scanning Calorimetry
EA	Elemental Analysis
FTIR	Fourier-Transform Infrared
GA	Glutaraldehyde
MCC	Microcrystalline Cellulose
NP	Nanoparticle
PVA	Polyvinyl Alcohol
SPION	Superparamagnetic Iron Oxide Nanoparticle
TGA	Thermogravimetric Analysis
UV	Ultraviolet
XRD	X Ray Diffraction

1 Context

In Portugal at the beginning of the 1990s, 18155 deaths could be attributed to malignant neoplasms, and in 2017 this number was closer to 30000 deaths. In fact, this rising trend is not unique in Portugal, since almost every country in the European Union has seen an increase in the incidence of malignant tumor and its related deaths [1], [2]. Although more people survive cancer nowadays due to advances in cancer research, a larger number of people will suffer from cancer as well, due to the increasing life expectancy [3]. Current cancer therapies like radiation and chemotherapy cause several negative side effects that significantly affect the patient's wellbeing, particularly in the lymphatic system, kidneys and heart, among others [4], [5]. Therefore, effective treatment with reduced side effects becomes a priority in cancer research. Hyperthermia is an ancient way of treating superficial tumors by applying heat to the affected region. Fast-forward a couple millennia and a different form of this therapy is being used: magnetic hyperthermia. Gilchrist *et al*. [6] in 1957 was the first group to use magnetic iron oxide nanoparticles for cancer treatments. Magnetic nanoparticles were injected into lymphatic channels producing heat when exposed to an alternating magnetic field, thus treating metastatic cancer.

Magnetic nanoparticles can be useful for biomedical applications for the already mentioned hyperthermia applications, but also for controlled drug delivery and imaging when using magnetic resonance [7]. Nevertheless, iron oxide nanoparticles face some limitations, with lack of colloidal stability being the main issue. This can be surpassed by coating the nanoparticles with a surfactant like oleic or dimercaptosuccinic acid (DMSA), avoiding their unwanted aggregation [8].

Cellulose nanocrystals (CNC) are also a nanomaterial receiving attention for its excellent properties, especially when it comes to biomedical applications like tissue engineering [9]. This interesting material is extracted from cellulose, the most abundant biopolymer in nature, and results in very attractive properties: biocompatibility, biodegradability and low toxicity. Nanocellulose-based materials can even be used as a stable environment for cellular growth, adhesion and proliferation: some studies have used cellulose nanowhiskers to grow oriented skeletal muscle cells while others used hydrogels to not only grow cells on the surface, but inside the scaffold as well [10]–[12].

Having this in mind, a previous work developed in the Soft and Biofunctional Materials Group (SBMG) combined the best characteristics of both iron oxide nanoparticles and cellulose nanocrystals in a hybrid composite [13]. The material's performance was tested in both magnetic hyperthermia and cytotoxicity assays. It was found that the nanoparticles granted CNC's better thermal properties. The films retained some degree of organization even with the presence of iron oxide nanoparticles, displaying iridescence. Although great results were achieved, it was found that the produced material was fragile, brittle and not easily manageable. This is relevant especially when the application is considered: after all, the material must withstand the physiological environment and minimal handling. Adding a polymer may be a viable path since it can make the composite more pliable.

Polyvinyl alcohol (PVA) is a non-toxic, biodegradable polymer already employed in drug delivery devices, hemodialysis and bio-separation membranes and soft contact lenses, and has already been used alongside cellulose nanocrystals since the latter is an efficient light-weight reinforcement [14]–[16].

Therefore, the goal in this work is to produce a ternary composite with PVA, a widely used polymer for medical devices; CNCs, a renewable and effective mechanical reinforcement; SPIONs, capable of generating heat when subjected to AMF. This composite should be biocompatible and able to generate heat, combining all the attractive properties of its constituents in one device for cancer treatment. To achieve this goal, the following objectives were proposed:

- Study the incorporation of the reinforcement material in the polymer matrix;
- Evaluate the maximum concentration of nanoparticles in the composite;
- Optimize the composites crosslinking taking into account the desired application;
- Assess the biocompatibility of the new materials through cytotoxicity assays;
- Evaluate the heating ability of the composites with magnetic hyperthermia tests;
- Characterize the composites with various techniques, including mechanical and water uptake tests to assess if they're appropriate for the physiological environment.

Four main parts will structure this work: firstly, there is a theoretical introduction to several relevant aspects of the composite and its functions. Secondly the materials and methods section will describe how and in which way the laboratory techniques were executed. After this, all the results will be presented and discussed. Finally, this work is finished with some final considerations, conclusions of the study and future perspectives.

2 Introduction

2.1 Magnetic Hyperthermia

The etymology of the word *hyperthermia* comes from the Greek and means “beyond temperature”. It is a millenary therapy used by ancient Greeks, Romans and Egyptians to treat breast masses with the first evidence being a papyrus dated from 3000 BC [17]. When it is intentionally applied to the human body, it causes the rise of temperature above the typical physiological temperature of 37 °C. Due to their abnormally fast growth, cancer cells have a defective vascular supply which makes them more susceptible to temperatures above 42 °C [18]. Different amounts of generated heat are required when the application is considered. For cancer cell death to occur, high heat generation is necessary; as opposed to the mild heat generation required for the activation of specific cellular targets, which bypasses the non-wanted side effects on other cellular components [19]. The mechanism by which cellular death happens is based on heat shock proteins, which alter the cellular walls. Hyperthermia also leads to lack of nutrients in the tumor cells, since it increases the oxygen supply, over-acidifying the cells. This increased temperature has the ability to damage, kill and make cancer cells more sensitive to subsequent treatments like radiation or other drugs [20], [21].

Hyperthermia ablation can be applied through microwaves, radiofrequency and high-intensity focused ultrasound but they face limitations: these can cause burns and other negative side effects that hinder their full potential [22]. An interesting mode of applying heat is through magnetic hyperthermia, where an alternating magnetic field is used to induce the temperature increase using magnetic field susceptible materials, like iron oxides nanoparticles. This is advantageous since iron oxide nanoparticles can be injected or applied on the cancer site, making it a location-specific treatment [23].

Magnetic spin relaxation is responsible for heat generation when it comes to small single-domain magnetic nanoparticles. The magnetization reversal process happens when an energy barrier is surpassed, and the magnetic nanoparticles are subjected to an alternating magnetic field. A certain amount of energy is required to rotate the magnetic nanoparticles away from their preferred direction. With repetitive alignments and relaxations of magnetic spins, heat is generated through energy dissipation. Néel relaxation happens with the flipping of the magnetic spins and is especially relevant when the nanoparticles are internalized and “fixed”. However, this is not the only way magnetic nanoparticles generate heat as depicted in Figure 2.1.

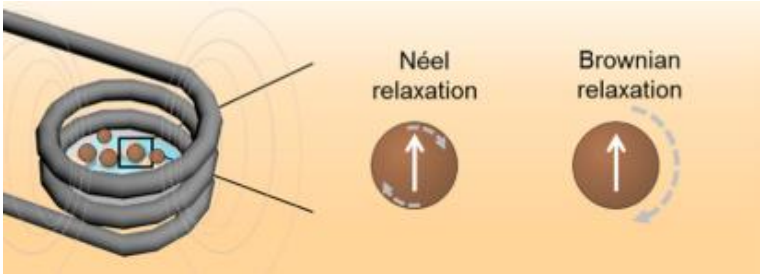

Figure 2.1 – Representation of Néel and Brown relaxation mechanisms. The brown circles represent the superparamagnetic iron oxide nanoparticles [19].

Brownian relaxation generates heat when whole particle relaxation occurs in a liquid by means of rotational friction, and the viscosity of a medium plays a part. In the case of a small particle, the effective magnetic relaxation time is dominated by the Néel relaxation; on the other hand, the bigger the particle, the more Brownian relaxation contributes to the effective magnetic relaxation time [19].

2.2 Superparamagnetic Iron Oxide Nanoparticles

The International Organization for Standardization (ISO) defines a nanoparticle as a material with all three dimensions in the nanoscale, this is, between 1 and 100 nanometers. Magnetic nanoparticles are a specific type of nanoparticles able to respond to a magnetic field, usually composed of an iron oxide, iron, cobalt or nickel core. Iron oxide nanoparticles are stable and biocompatible and when superparamagnetic, are called SPIONs (superparamagnetic iron oxide nanoparticles), being widely used for biomedical research in recent years. Various techniques can be employed to produce iron oxide nanoparticles including coprecipitation, thermal decomposition, sol-gel and hydrothermal reaction. Chemical coprecipitation is a widely used method to produce iron oxide nanoparticles because it is a simple, fast and low-cost technique. By tailoring the reaction parameters, it is possible to achieve a precise control over the nanoparticle size, which is critical for superparamagnetism to occur. This special behavior means that the magnetite nanoparticles display a single magnetic dipole and magnetic momentum, which does not happen to the same material in greater than 30 nm dimensions. In practical terms, small magnetic nanoparticles are only magnetized when a magnetic field is being applied, which is especially useful for drug delivery applications, since nanoparticles can be guided through the body to the tumor site and control the drug delivery [24]. They are also used for other biomedical applications like enhanced imaging through magnetic resonance, tissue repair, and cell/tissue targeting [25].

It is therefore expected for biosafety to be an important issue when regarding iron oxide nanoparticles for biomedical applications. It is crucial to know what kind of interactions they have with cells, proteins, etc., but also how they affect essential life mechanisms. One other aspect when considering the biosafety of SPIONs is how they biodegrade within the body and their possible bioaccumulation. This is an aspect where the surface groups of the SPIONs are important since some studies have stated that bare SPIONs are toxic [26]. Coatings are also useful to prevent aggregation issues and to link bioactive components, like drugs [27]. Besides natural polysaccharide coatings like the usual dextran, synthetic polymer coatings are also an option to improve these magnetic nanoparticles biocompatibility [19]. *Meso*-2,3-dimercaptosuccinic acid is widely used to coat magnetite nanoparticles. DMSA is widely used to coat SPIONs and produce a water-stable nanoparticle suspension in a wide range of pH values. Not only does it improve their stability but also the biocompatibility and internalization, making the nanoparticles less cytotoxic when compared to their non-coated counterparts [28].

2.3 Cellulose Nanocrystals

With the recent years' climate change and depletion of natural materials resources, cellulose emerges as one of the top raw materials, being the most abundant biopolymer, simultaneously renewable, biocompatible and biodegradable. It can be found in plants' cell walls, algae and some bacteria,

composed by its repetitive unit, cellobiose. This monomer is made up of two units of anhydroglucopyranose alternately rotated 180° linked into linear chains by 1,4-β-glycosidic bonds [29].

Cellulose nanocrystals have an anisotropic nanorod appearance and can be obtained through the strong acid hydrolysis of cellulose fibers. The acid cleaves the more susceptible amorphous regions between the crystalline sections, leaving only the CNC nanorods as seen on Figure 2.2 [30]. These can have 50 to 1160 nm in length and range from 3 to 50 nm in diameter, which strongly depends on the hydrolysis conditions and origin of cellulose [31]. CNCs also present high axial stiffness and tensile strength, low density and good thermal stability [32]. When produced with sulfuric acid, the formed sulfate ester groups result in negative charges on the surface of the CNCs, enhancing their stability in water due to the electrostatic repulsion [31], [33], [34]. If suspended in water at low concentrations, they will self-assemble into a left-hand lyotropic cholesteric phase. Producing a film from this suspension by full solvent evaporation, will result in a photonic material that presents a short pitch (few hundreds of nanometers), and structural coloration, related to the wavelength of light in the visible region of the electromagnetic spectrum. Through this mechanism, photonically attractive structures can be produced, displaying iridescence and selective circularly polarized light reflection, being even used in security labeling, cosmetics and coatings [33], [35]. CNCs have received growing attention in recent years, especially when it comes to their biomedical applications. Some interesting works also showed that organized structures like liquid crystalline phases or even spin-coated membranes of cellulose nanowhiskers extracted from tunicates show the ability to grow oriented muscle cells [10], [36].

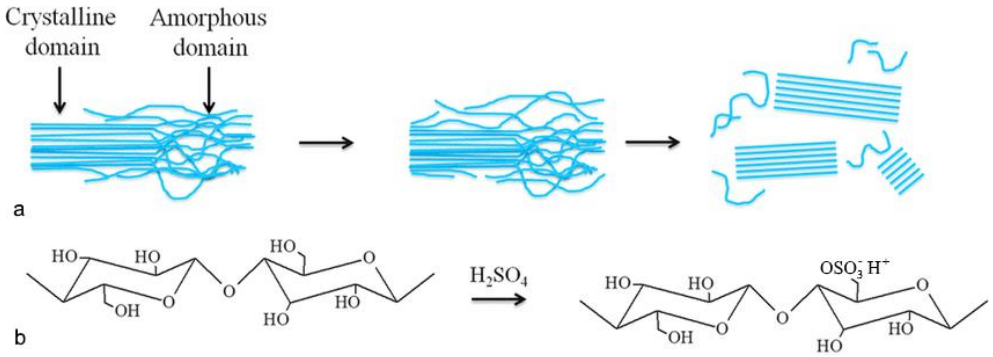

Figure 2.2 - Representation of a) cellulose fibers, where the crystalline and amorphous regions are depicted, b) cellobiose, the repetitive dimer of the polymer cellulose and the effect of sulfuric acid hydrolysis in the polymer adapted from [37].

2.4 Polyvinyl Alcohol

Applications of polyvinyl alcohol can be found in almost every industry sector. Considering its biomedical applications, it has been made into contact lenses, artificial organs, sensors, membranes, artificial cartilage, wound healing, tissue engineering scaffolds and drug delivery systems [38]. One interesting aspect of this material is the possibility to make stimuli-responsive hydrogels in which the water uptake depends on environmental conditions like pH, temperature, magnetic fields, and so on. This trend is justified by the comparable properties of hydrogels and human tissues regarding the retained amount of water and low interfacial tension with fluids [39]. PVA has good thermal and pH stability, it is widely available, inexpensive, nontoxic, biocompatible, easily-processed, and hydrophilic [40]. Because

of its hydrophilic nature, it must be modified to minimize swelling in water [41]. This modification to improve mechanical integrity can include freezing, heat treatment, irradiation and chemical crosslinking. Regarding chemical crosslinking, there are numerous crosslinking agents that enable the reaction with glutaraldehyde and citric acid being the most common (Figure 2.3) [42]. Citric acid is an advantageous crosslinker as it is already used as a low-cost food additive (E330) and crosslinking agent for compounds with hydroxyl groups (see Figure 2.3) [14], [43]. Being a metabolic product of the body, it is expected to be biocompatible [15]. The crosslinking with PVA happens through an esterification reaction between the carboxyl groups in citric acid, and the hydroxyl groups in both PVA and CNC, making it a double efficient crosslinker [42], [44]. Wang *et al*. [45] produced a novel packaging material with PVA and xylan, a polysaccharide and type of hemicellulose. This group found that the interactions between both polymers were enhanced by the presence of citric acid, with hydrogen and ester bonds forming between the components.

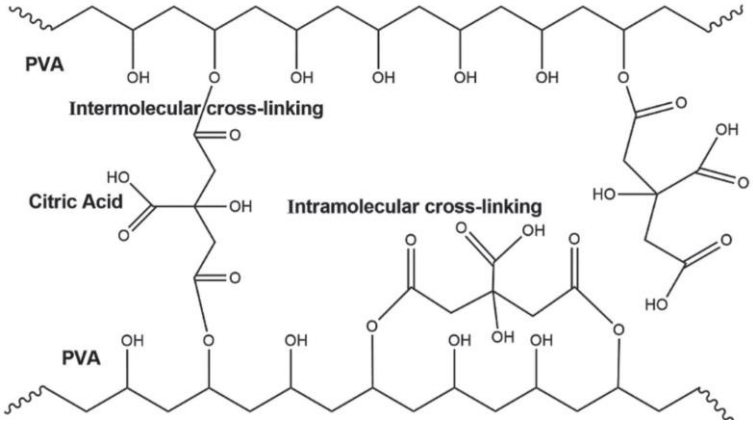

Figure 2.3 -Reaction scheme showing both intermolecular and intramolecular crosslinking of PVA using citric acid [46].

Glutaraldehyde reacts with PVA's -OH functional groups, creating acetal bridges and resulting in a sort of net that is characteristic of crosslinked polymers [39]. Figure 2.4 represents this reaction. Since the hydrophilic -OH groups are consumed in the crosslinking process, an optimum degree of crosslinking is favorable [41]. When using GA, acidic conditions catalyze the acetalization of hydroxyl and aldehydic groups. Hydrochloric acid may be a good candidate since it is volatile and will not leave residues that can tamper with the other reagents. Although glutaraldehyde is accessible, economical and effective, it is toxic and must be neutralized [47].

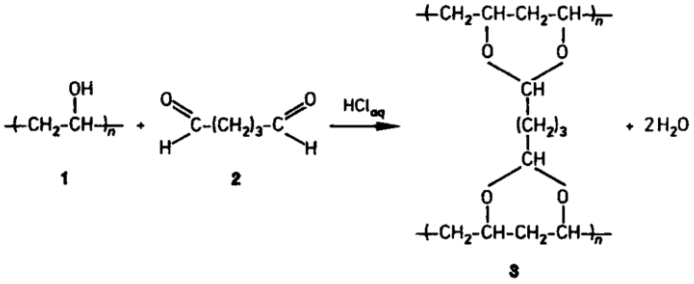

Figure 2.4 - Reaction between PVA (1) and GA (2) in acid conditions provided by hydrochloric acid, resulting in crosslinked PVA by acetal bridges (3) with the release of water [48].

2.5 Composite's state of the art

In 2004 Lao *et al*. [49] dispersed magnetic microparticles (Fe_3O_4) in a polyvinyl alcohol hydrogel and studied the hybrid material's potential for hyperthermia, having achieved a stable maximum temperature between 43 and 47 °C within 5 to 6 min. The research group crosslinked this hydrogel via freeze and thaw method. Being a physical crosslinking method, it excuses the usage of chemical crosslinkers; however, it is very time-consuming since it can take at least 3 days. They found that the maximum temperature was a function of the Fe_3O_4 concentration. Other processes can be less time consuming regarding the crosslinking of a hydrogel. One can choose a chemical crosslinker, like glutaraldehyde. Twelve years later, Tanpichai *et al*. reinforced glutaraldehyde crosslinked PVA hydrogels with 1 wt.% CNC and found that the compressive strength was greatly increased. In fact, CNC makes for a great reinforcement due to their high strength and elasticity modulus. A better strain recovery was found as well in the reinforced samples, and it was found that this addition did not affect the swelling ratio or thermal stability of the hydrogels [50], [51].

In their 2013 work, N. Rescignano *et al.* [52] proposed a ternary bio-nanocomposite using PVA, cellulose nanocrystals and PLGA nanoparticles, with the goal of drug-delivery. The incorporation of 0.5 % of CNC increased the elongation properties without jeopardizing the other mechanical properties. Furthermore, CNCs can also be used to orient particles in a hydrogel: just 3 years later Yoshitake *et al.* [53] developed a gelatinous-composite from iron oxide nanoparticles and t-carrageenan while using CNC to orient the magnetic nanoparticles in the film. The group observed a specific response in drawn/pulled films to an external magnetic stimulus, attributed to the magneto-anisotropy of the preferred orientation of the iron oxide particle aggregates. Nonetheless, Shen *et al*. [54] were the only research group to have joined magnetite nanoparticles, cellulose (microcrystalline) and polyvinyl alcohol in a composite. This work was published in 2018 and resulted in an aerogel for dye removal produced in an eco-friendly manner. The article pertinently remarks that there are relatively few studies devoted to developing cellulose and PVA composites as matrix for supporting the NPs. Some groups have combined nanocellulose and non-iron-oxide-metallic nanoparticles in polyvinyl alcohol for hyperthermia [55], but also for other purposes, like antimicrobial applications. Zhong *et al.* developed antimicrobial polyvinyl alcohol films reinforced with hybrid cellulose-copper nanoparticles, while Xu *et al.* created CNC/silver-NPs functional fillers and produced a PVA blend membrane effective against Escherichia coli and Staphylococcus aureus [56], [57]. To date, the combination of CNCs, SPIONs and PVA has not been reported in literature. In this work, this novel composite is extensively studied and characterized for biomedical applications.

3 Materials and Methods

3.1 Synthesis of cellulose nanocrystals

The reagents utilized in the synthesis of cellulose nanocrystals and its procedure, are described elsewhere [58]. To increase the concentration of CNC in the final suspension, a 15 % PEG aqueous solution was prepared, and the CNC suspension was introduced into a dialysis tubing (SnakeSkin™ with 3.5 K of molecular weight cut-off and 35 mm dry internal diameter membrane) and left in dialysis overnight against the PEG solution, reaching a concentration of 6.64 ± 0.55 wt.% determined by gravimetric method with 7 replicas. The suspension was stored at 4 °C to avoid degradation and bacterial or fungal growth [29].

To improve the stability of CNCs and increase its initial pH (initial value of 1.59), the proton on the ester sulfate group that are present on the surface of CNC's was exchanged to Na^+ with an ion-exchange resin. The resin Amberlite® IR120 in the hydrogen form (by Sigma Aldrich), was washed in ultrapure water three times. Afterwards a 10 wt.% NaCl aqueous solution was put in contact with the resin, so the exchange of the ion H^+ to Na^+ would occur. Since HCl is formed, the pH was measured and monitored until it was no longer acidic, which indicated the complete exchange. The resin was placed in the CNCs suspension for a week, and a final pH value of 4.6 was achieved. The presence of Na^+ was determined by Inductivity Coupled Plasma Atomic Emission Spectroscopy (ICP-AES) as described in Supporting Information.

3.2 Iron Oxide Nanoparticles Synthesis

Iron oxide nanoparticles were synthesized by chemical co-precipitation method as described elsewhere [59]. The magnetic nanoparticles were stabilized using dimercaptosuccinic acid.

3.3 Ternary Composite

A 10 wt.% solution of PVA (95 % hydrolyzed, average M.W. 95,000, Acros Organics) was prepared by dissolving the PVA in ultrapure water with magnetic agitation (500 rpm) in an oil bath at 90 °C, during 1 h until the polymer was visibly dissolved and left to cool. The solution was stored in the fridge for the above-mentioned reasons.

Three types of mixtures were made for each of the crosslinking agents. PVA, PVA with CNCs (PVA/CNC) and PVA with both CNCs and Fe_3O_4 nanoparticles (PVA/CNC/NP). Glutaraldehyde and citric acid were used as crosslinkers (5 % m/m in respect to PVA) and hydrochloric acid as a catalyst (2 % wt.) in the glutaraldehyde samples. Hydrochloric acid/glutaraldehyde mixtures were prepared in advance and stored in the fridge. For simple PVA samples, PVA was submitted to magnetic stirring and the crosslinker/catalyst solution was added. The mixture was poured into polystyrene Petri dishes (55 mm of diameter). For the citric acid crosslinked solutions, they were put overnight in an oven at 60 °C, to evaporate water and produce manageable films. In the case of glutaraldehyde crosslinked samples, they were left to dry uncovered at room temperature. In PVA/CNC samples, a 0.5 wt.% amount of CNCs were added with respect to the PVA content. Membranes were obtained as described above

for the pristine PVA samples. In PVA/CNC/NP samples, the amount of nanoparticle suspension was added after the CNCs, in order to make 10 wt.% of the PVA content. The citric acid containing samples were submitted to a thermal treatment at 130 ºC for 5 h for best crosslinking results. All samples were washed with PBS and ultrapure water in order to wash out any acidic (CA or HCl) residues.

3.4 Water Uptake tests

To evaluate the water uptake capability of the hydrogels, the weight swelling ratio of the samples was analyzed. 10x10 mm squares were cut from the samples PVA, PVA/CNC and PVA/CNC/NP with 3 replicas each. These were put in the oven until dry, reaching the final dimensions of 5x5 mm. For the samples where citric acid was used as a crosslinking agent, 5x5 mm squares were cut.

3.5 *In vitro* tests

Being the goal of this composite its biomedical applications, it is essential to assess its toxicity to cells. Cytotoxicity assays were employed following the extract method and the norm *ISO 10993 – Biological evaluation of medical devices, Part 5: Tests for in vitro cytotoxicity and Part 12: Sample preparation and reference materials*. Cell adhesion and proliferation assays were done as well. These procedures are described in more detail in section 7.3.1 of Supporting Information.

3.6 Magnetic Hyperthermia

The thermal behavior of the nanoparticle-containing samples was analyzed with *Nb Nanoscale Biomagnetics' DM100* Series equipment. The used parameters were 10 minutes, 418.5 kHz of frequency and 24 $kA.m^{-1}$ of magnetic field strength.

3.7 Mechanical Tests

A Hegewald & Peschke inspect micro LC100N equipment was used, with a 100 N load cell. The tests were run with a speed of 2 mm/min and until break or reaching 95 N of load. For tensile tests, 3 replicas were used, and the CA-crosslinked samples were cut in 5x20 mm rectangles (gauge length of 10 mm) with average thickness of 428, 592.5 and 732.5 µm for the PVA, PVA/CNC and PVA/CNC/NP dry samples, respectively. The hydrogel samples were cut in 5 mm diameter circles with half a millimeter of thickness in the case of PVA/GA and PVA/CNC/GA and 1.5 mm for PVA/CNC/NP/GA, tested after extraction from water and patted dry. In the case of compression, 10 replicas were used, and the sample was set on the lower plate and elevated until in contact with the top plate and a preload force of 0.1 N was set to guarantee full contact between the plates and the sample. The compressive modulus was calculated between 10 and 20 % strain and assumed as the compressive modulus for 15% of strain.

3.8 Characterization

All the specifications and parameters used in the various characterization techniques employed in the thesis are described in section 7.4 of Supporting Information.

4 Results and discussion

This work is focused on the optimization and characterization of a novel ternary composite for magnetic hyperthermia applications, incorporating three promising materials: cellulose nanocrystals, Fe_3O_4 superparamagnetic nanoparticles and polyvinyl alcohol.

The first part of the work delves into the synthesis of cellulose nanocrystals from microcrystalline cellulose and its sodium treatment, being subsequently used in the production of both iridescent films and ternary composites. These underwent morphological, structural and chemical characterization. Adhesion and proliferation tests were completed with the composite material previously developed by the SBMG, a hybrid composite of CNCs and SPIONs. After this, a new formulation for this material was proposed. The well-studied magnetic nanoparticles were produced via chemical co-precipitation method and incorporated in a PVA matrix. This incorporation was also tested for the cellulose nanocrystals. After this, a study of the crosslinking of the new ternary composite was performed.

Besides structural and chemical characterization of the composites, water uptake tests were performed to understand the materials' behavior in aqueous environments, magnetic hyperthermia tests were carried out to measure the material's heating ability, and cytotoxicity assays were executed to assess the biocompatibility of the novel composites.

4.1 Cellulose nanocrystals' production

The first part of this thesis focused on the production of cellulose nanocrystals as described elsewhere [58]. One of the detected problems with the CNCs produced by this methodology was their low pH after synthesis, around 1.59. To make them more suitable for biomedical applications the pH should be around 7, however previous studies have showed that this value did not allow to retain the liquid crystalline organization of the CNCs in suspension [13]. So, CNCs were treated with an ion exchange resin containing sodium (Na^+) ions for a week (adapted from [60]). pH values were continuously measured, and resin was progressively added as needed. The effectiveness of the ion exchange was verified by the obvious increase in pH but also by Inductively Coupled Plasma – Atomic Emission Spectroscopy (ICP-AES). As a result, CNCs suspension increased the pH up to 4.6. This step is important since the lowering of the acidity can avoid degradation and guarantee better biocompatibility results.

The amount of carbon, hydrogen, nitrogen and sulfur was determined through elemental analysis (EA), with 2 replicas for each sample. The results are summarized in Table 4.1, with oxygen values being calculated by difference. The presence of sulfur in the CNC sample is expected and is attributed to the addition of sulfate half-ester groups during the sulfuric acid hydrolysis of microcrystalline cellulose, indicating an effective acid hydrolysis [61].

The obtained numbers can be very useful to calculate the incorporation of sulfate half esters into the surface of the CNCs. The method to do so has been previously reported by Hamad *et al.* [61], and it allows the determination of the degree of substitution (n) of hydroxyl groups by-OSO_3H groups per hundred anhydroglucose units (AGU). This value is calculated by the following equation:

$$S\,(\%) = 100n \times \frac{S}{6C + 10H + (5+3n)O + nS}$$ Equation 4.1

The amount of sulfur and calculated n value was 5.35 -OSO_3H per 100 AGU units for the experimental acid hydrolysis conditions used. For the same experimental conditions Fernandes *et al*. stated a 0.85 wt. % of sulfur content and subsequently a n value of 4.39. The observed difference is within the elemental analysis' error, and it is therefore in accordance with the literature [58].

ICP-AES analysis determined a sodium concentration of 63.1 mg/L, confirming the efficient sodium substitution of H^+ (nitric acid showed a value of 3.86 mg/L, for reference). The substitution mechanism is pictured in Figure 4.1. Relative percentages of sulfur and sodium in the sample could be calculated, although the resolution's limit of EA and ICP-AES are different and could lead to inconsistencies. Thus, both elements should be analyzed via ICP-AES though it should be noted that the latter is a much more expensive technique.

Table 4.1 – Values of the elements C, N, H and S detected by elemental analysis on the precursor, final CNC material and values predicted for pure cellulose. The values are presented in percentage; the amount of oxygen (*) was calculated by difference.

	C	**N**	**H**	**S**	**O***
Pure celulose [62] (predicted values)	44.44	0	6.18	0	49.38
Microcrystalline cellulose	43.51	0	6.42	0	50.07
Cellulose nanocrystals	41.14	0	6.05	1.03	51.78

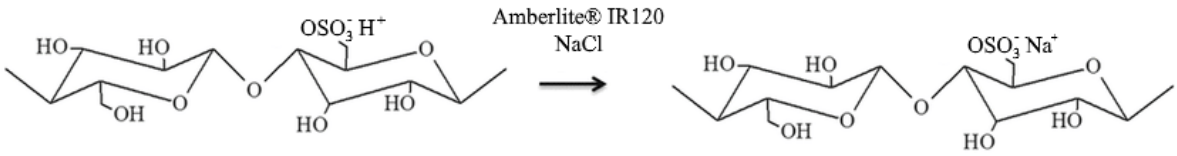

Figure 4.1 - Diagram of H+ to Na+ proton substitution in CNCs after contact in Na protonated ion-exchange resin

ATR-FTIR enabled the chemical analysis of the cellulosic samples, and the obtained spectra of the precursor material (microcrystalline cellulose), CNCs and sodium CNCs are presented in Figure 4.2. There are four characteristic IR absorption frequencies attributed to cellulose's functional groups: the stretching vibration of the O-H bond at 3339 cm^{-1}; the stretching vibration of C-H at 2900 cm^{-1} bond and C-O at 1054 cm^{-1}; and bending of O-H bond at 1650 cm^{-1}. After acid hydrolysis, -OSO_3H groups substitute some of the -OH groups, resulting in a band at 780-860 cm^{-1} range due to the S-O stretching. No differences are seen when comparing CNC with the proton ion and sodium protonated CNC. This analysis indicates that CNC Na presents the same chemical linkages as cellulose. All the identifications are in accordance with the values found in literature [63].

One expects that the acid hydrolysis process will not influence the structural organization of the cellulose, however it should induce an increase in crystallinity of the sample since it will remove preferentially the amorphous regions of the cellulosic fibers. CNCs crystalline structure was analyzed by XRD by comparing the results from the precursor material, CNCs and CNCs treated with sodium (Figure 4.3).

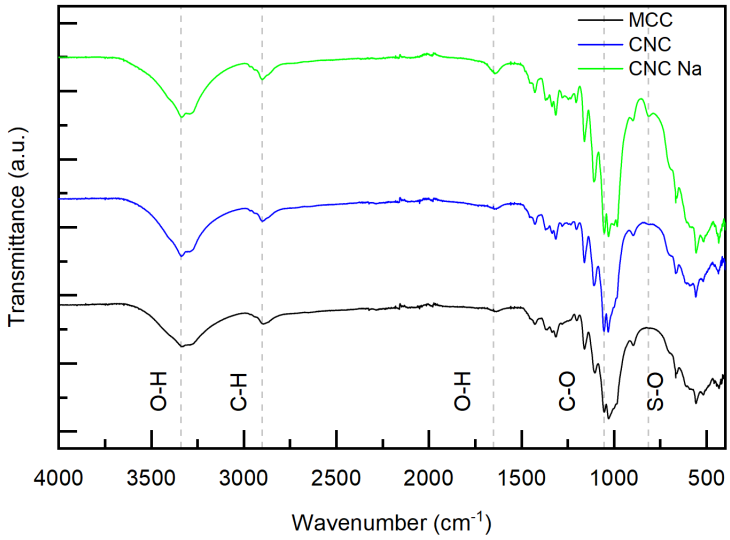

Figure 4.2 – ATR-FTIR spectrograms of the precursor material - MCC, CNC and sodium CNCs (CNC Na).

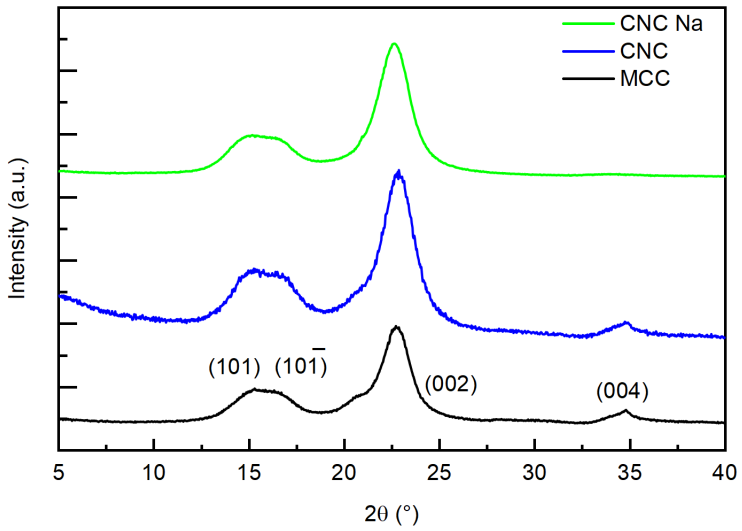

Figure 4.3 - XRD diffractograms of the precursor material - MCC, CNC and sodium treated CNCs (CNC Na).

XRD diffractograms present the peaks of the type I allomorph cellulose confirming that the hydrolysis process does not affect the structure of cellulose. In order to infer if the reaction changes the crystallinity of the sample, crystallinity “indexes” were calculated with a method presented by Segal *et al.* [64] , in which one divides the difference between (002) peak’s height and the minimum value between 18 ° and 20 ° by the (002) peak’s height:

$$I_c = \left(\frac{I_{(002)} - I_{am}}{I_{(002)}} \right) \times 100$$ Equation 4.2

When analyzing the diffractograms, the most obvious peak is (002) at 22.6 °, surrounded by other smaller and subtle peaks at (101), ($10\bar{1}$) and (004), at 15°, 16.8° and 34.9°, respectively. These results confirm that the hydrolytic process does not alter the cellulose nanocrystals' structural organization, since they are characteristic of native cellulose, and present in all three samples. The results are within expectations and relevant literature [63].

CNCs presented a crystallinity "index" of 92.1 % while the precursor material, microcrystalline cellulose, showed an 88.24 % crystallinity "index", confirming the removal of amorphous regions. CNC Na exhibited a 92.5% value in respect of "index" of crystallinity. Although this value is higher than the one obtained for CNC, it should be noted that this shift is probably related to the method to determine the index, and not the material itself, since it has not suffered any process that would affect its crystallinity.

The morphology of CNCs was visualized by AFM images, as can be seen by the topographic scan (Figure 4.4 a), and the dimensions of 200 nanoparticles were measured from the images. From this it was possible to obtain the length and width distribution curves, Fig. 4.3 b and c, respectively. From this analysis, the length and width of the nanoparticles were determined as 138 ± 49 nm and 5 ± 1 nm respectively leading to an aspect ratio of 27. These results indicate a successful hydrolysis process and are in agreement with the literature [65].

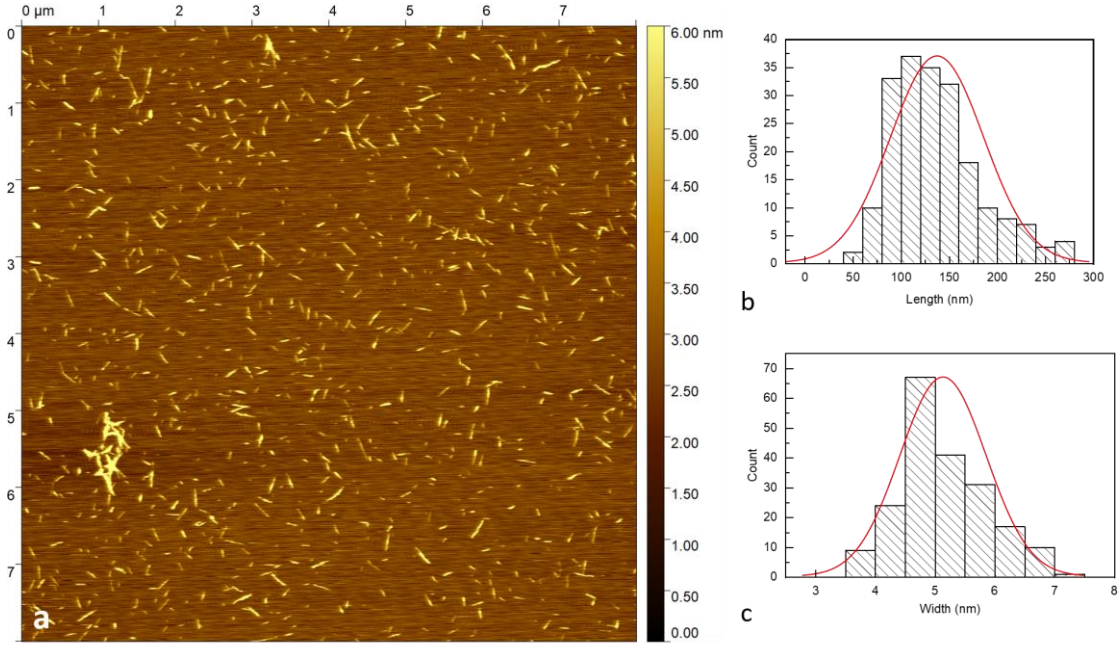

Figure 4.4 – AFM-acquired topographic image, in amplitude mode, showing individualized CNC, and the respective distribution of measurements regarding length and width of the nanocrystals.

Differential thermal analysis was performed on microcrystalline cellulose, CNCs and sodium protonated CNCs, through both thermogravimetric (TGA) and simultaneously differential scanning calorimetry measurements. Both TGA and DSC curves for the three cellulosic samples are presented in Figure 4.5, in panels a) and b), respectively. When a material is subjected to thermogravimetric analysis, it is

decomposed by heat, and the bonds within molecules are broken. This technique can be useful when assessing the thermal stability of materials. The first decrease in mass, observed for all samples until 100-130 °C is usually attributed to evaporation of water and residual moisture in the samples. Several degradation mechanisms like decomposition, dehydration and depolymerization of glycoside units are triggered in the 150-350 °C range. For microcrystalline cellulose, an abrupt loss of mass is noticeable between 285 °C and 345 °C, followed by a much slower and gradual decrease in mass until the end of the experiment, concordant with the trend usually seen in pure cellulose. This follows a first order degradation trend, typical of cellulose pyrolysis [66].

Focusing on CNC and CNC Na curves, it can be seen that both samples experience an accentuated loss of mass at 145 °C and 205 °C, respectively. When comparing CNC Na with its counterpart, a 50 °C improvement in thermal endurance is noticeable. This is attributed to the already reported improved thermal stability seen in neutralized and basic pH CNCs These two curves show another fall, although smaller, around 275 °C, until the end of the test, where about 30 % of the initial mass is left. The steadier feature of these curves when compared to the sudden drop of MCC can be attributed to the presence of sulfate groups, preventing the would-be two-step reaction. This presence also explains the higher amount of residue at the end of test: sulfate groups facilitate the extraction of water from the structure, dehydrating it and leading to a subsequent loss of oxygen. With no oxygen, the main mechanism of mass loss during pyrolysis is avoided, with no emission of CO and CO_2, preventing mass loss [66].

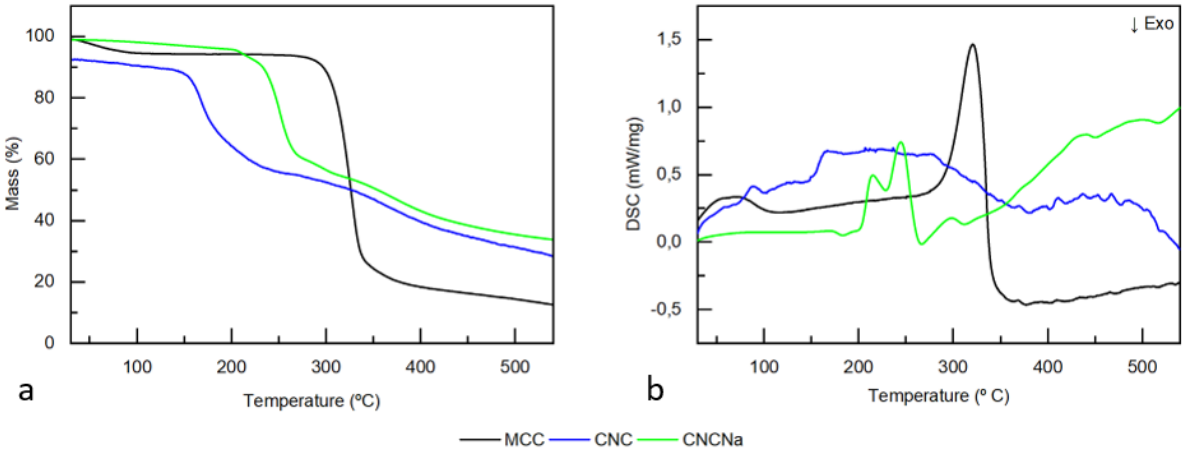

Figure 4.5 – Differential thermal analysis of microcrystalline cellulose, CNC, and sodium protonated CNC. a) the graph for thermogravimetric measurements. b) the differential scanning calorimetry analysis is presented.

Regarding differential scanning calorimetry, CNC Na presents two smaller endothermic peaks around 230 °C and a single more intense peak at 320 °C for MCC, confirming the significant mass losses already mentioned above. The CNC samples do not present this kind of behavior, indicating a gradual loss of mass, which mirrors the slow and multiple-step degradation of the cellulose chains and sulfate derivatives [62], [66].

4.2 Hybrid composite system – preliminary work

A previous work developed in the Soft and Biofunctional Materials Group (SBMG) combined both superparamagnetic iron oxide nanoparticles and cellulose nanocrystals to produce a novel hybrid composite for biomedical applications [13]. Taking advantage of the self-assembly of CNCs into a liquid crystalline phase, the cholesteric organization can be retained upon solvent evaporation and iridescent films were produced with and without SPIONs. The mixture between the two materials was optimized resulting in a final composition of 4 wt.% CNC suspension, and 3 wt. % of SPIONs (in respect to CNC mass). The films retained the cholesteric organization observed for the suspension even with the presence of SPIONs (seen in Figure 4.6). This new composite material was tested in magnetic hyperthermia application resulting in a temperature increase of about 1.5 °C. Additionally, none of the materials tested positive for toxicity by the extract method [13]. Although the group has shown that the produced materials are non-toxic, no information regarding cell proliferation was done, so these tests were performed in the present thesis. In order to do so, it was necessary to produce new materials. Similar iridescent films (without SPIONs) using the CNC treated with sodium were prepared as described in detail in section 7.1 of Supporting Information, with the final result pictured in Figure 4.7.

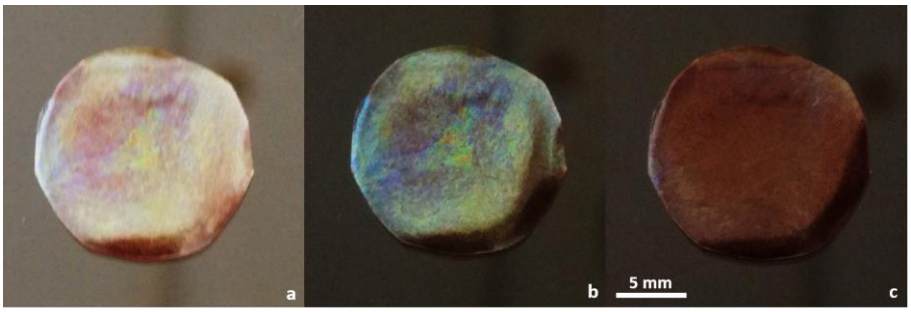

Figure 4.6 - Photographs of hybrid CNC and SPION films previously produced by the SBMG. a) No polarizer b) left circular polarizer c) right circular polarizer. Same scale applies to all of the images in the composition.

These iridescent films with 100 μm of thickness present selective reflection of circularly polarized light. This phenomenon indicates that the cholesteric organization is maintained even after full evaporation of the solvent. Since CNCs self-assemble themselves (in water, at low enough concentrations) into a left-handed chiral nematic phase, only left circularly polarized light is reflected. This is confirmed by the photographs as seen in panels b) and e). In panels c) and f) it's possible to see the extinction of transmitted right circularly polarized light.

Following, superparamagnetic iron oxide nanoparticles were prepared by chemical co-precipitation technique previously optimized by [59], coated with DMSA due to their low stability in physiological conditions, and extensively characterized in a recent study [8]. Figure 4.8 shows the most representative results of SPIONs characterization. To offer some context, the study shows that the uncoated iron oxide nanoparticles are spherical with an average diameter of 9.4 ± 2 nm (when observed by TEM). DMSA coating does not affect the morphology or average diameter. When it comes to its crystallinity, nanoparticles were characterized via XRD, having been possible to observe the characteristic peaks of magnetite's cubic crystalline structure. The surfactant's presence didn't affect the crystallinity in any way. The

dynamic light scattering measurements, employed to assess their stability, showed that are two groups of nanoparticles, classified by its average diameter: 164 ± 13 nm e 101 ± 9 nm.

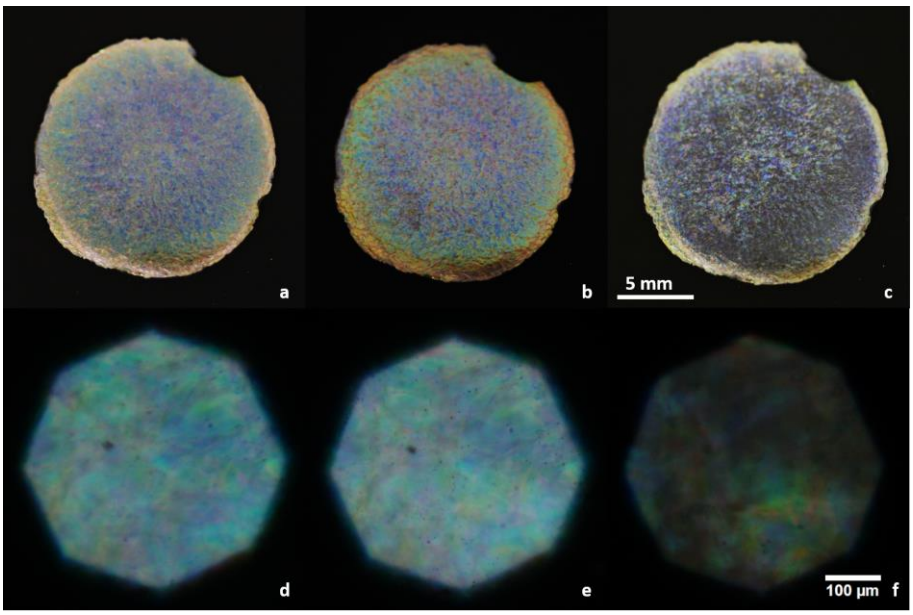

Figure 4.7 - Film made from sodium treated CNCs by full solvent evaporation at 37 °C. Photographs of said film: a) unpolarized white light b) left circular polarizer c) right circular polarizer. d), e) and f) are polarized optical microscopy images of the same films.

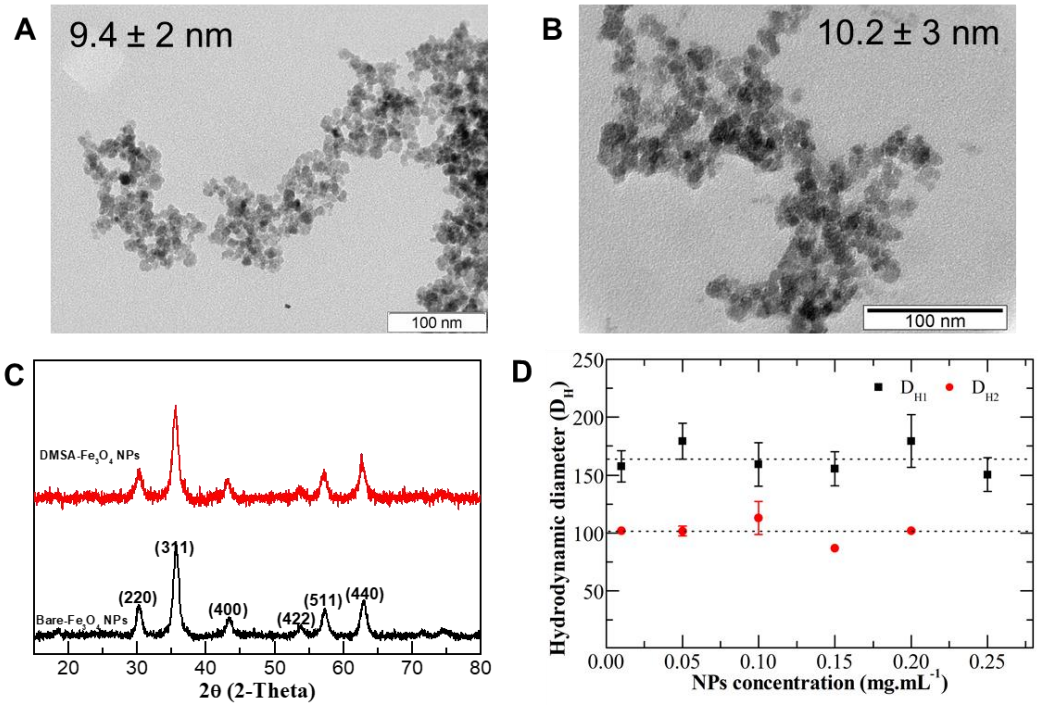

Figure 4.8 –SPIONs characterization: A) TEM image of bare Fe_3O_4 NPs B) TEM image of DMSA-coated Fe_3O_4 NPs C) XRD spectra of both bare and DMSA-coated Fe_3O_4 NPs D) Hydrodynamic diameters of DMSA-coated Fe_3O_4 NPs [8].

Using the CNC-Na and SPIONs, hybrid films were produced with a final composition of 4 wt.% CNC-Na suspension, and 3 wt. % of SPIONs (in respect to CNC mass). Similarly to what was observed for

the CNC films, these retained the helicoidal structural organization derived from the liquid crystalline suspensions of CNCs, which might influence cell growth. To test this hypothesis, adhesion and proliferation *in vitro* tests were completed to evaluate the performance of the hybrid composite system. Figure 4.9 represents the adhesion and proliferation of Vero cells on CNC and CNC/NP films with cell viability as a function of the number of days. Analyzing the results of relative viability (Figure 4.9) for the CNC films, it is possible to notice the prolific growth from the first to the third day, accompanying the trend of cell control. It is followed by a fall in number of cells on the sixth day and subsequent growth until the last time point. For the material containing SPIONs, throughout six days the growth is in accordance with cell control values, demonstrating a fall on the fourth time point (eight and a half days). On the last day, it is noticeable that the growing process recovered. Regarding the cell control values, they are all as predicted although the last day presents a setback, with a lower count of cells when compared to the previous time point. However, these three punctual falls in cell count do not indicate a lack of cell proliferation, but rather human errors, like possible aspiration of cells.

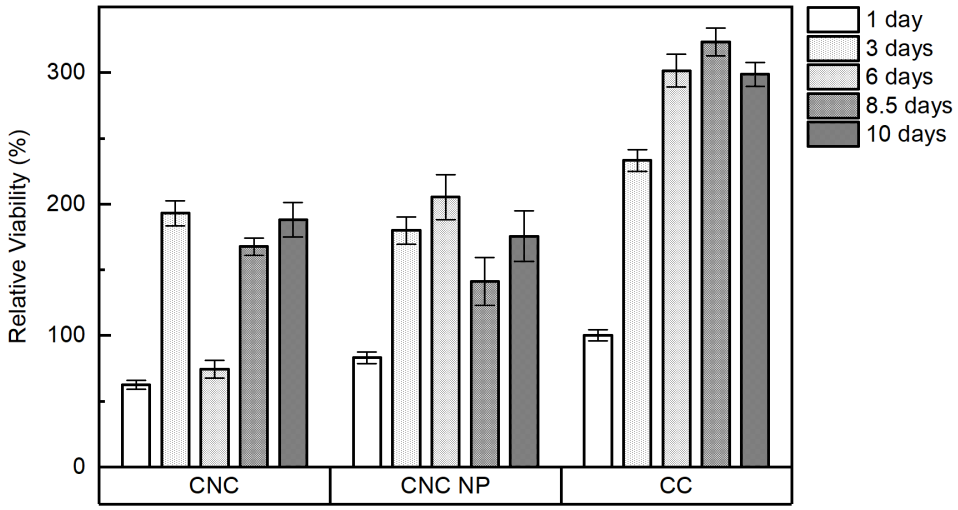

Figure 4.9 - Adhesion and proliferation of Vero cells on CNC and CNC/NP films throughout 10 days measured using the resazurin method. The last column, CC, refers to the cell control.

Dye staining was employed in Vero cells from the adhesion and proliferation test enabling their observation using Phalloidin (red coloration in the images) stains actin, a constituent of the cytoskeleton of cells; DAPI (4',6-diamidino-2-phenylindole, dihydrochloride) stains the cell's nuclei, visible in blue in the pictures in Figure 4.10. When comparing all three images, it is possible to assess that the first is more confluent – this is because it concerns the cells in the control well, which are in greater number. Nonetheless, all images confirm the good health of cells in contact with the tested materials.

The obtained results from adhesion and proliferation tests demonstrated promising results concerning cell adhesion in the hybrid material of CNC/SPIONs. Even though cell proliferation was demonstrated in the preliminary tests, no influence of the CNC organization was detected. A lower cell count may be needed in order to infer on the orientation of the cells on top of the films. Additionally, it is important to note that the final hybrid composite system was extremely fragile, brittle and not easily manageable. Since this hybrid composite material was developed for biomedical applications, the final

structure must endure the physiological environment and minimal handling and therefore it must be optimized.

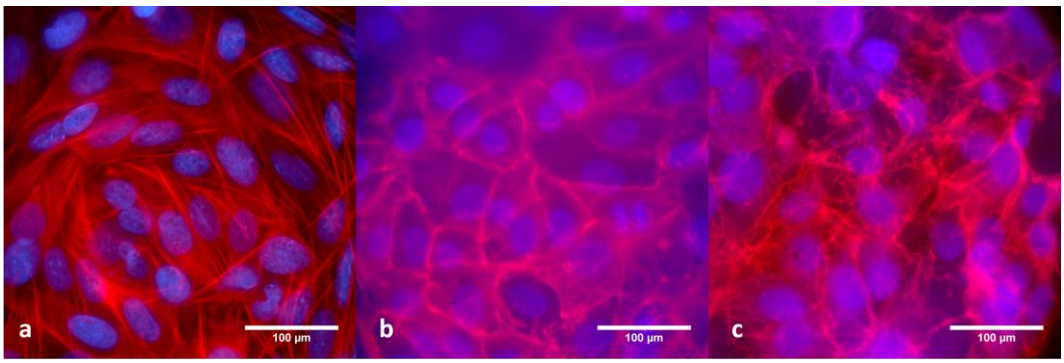

Figure 4.10 – Fluorescence microscopy images from Microscope Nikon Eclipse Ti-S of a) control cells, b) cells adhered to CNC films and c) cells adhered to CNC/SPIONs films. Cell's cytoskeleton is visible in red and the nuclei in blue.

From these preliminary results, a new structure was designed to incorporate CNCs and SPIONs while improving the flexibility of the composite hybrid system. It is well known from literature that CNCs are used as mechanical reinforcements in several types of composites [51], [67], [68]. Therefore, to obtain a more pliable and manageable material, polyvinyl alcohol was used as a matrix. In this work we attempt to associate and optimize CNCs and SPIONs in PVA and study its mechanical improvements, biocompatibility and magnetic hyperthermia ability.

4.3 Hybrid composite system production

To produce the hybrid composite system, three core materials were used: CNCs, SPIONs, and PVA as matrix. 10 wt.% PVA solution was produced, since this is a widely used and convenient concentration to use by the scientific community [52]; a suspension of sodium-treated CNCs and DMSA-coated SPIONs were used, the latter chosen based on their already extensively studied stability and heating capacity qualities. Different amounts of CNCs and SPIONs were incorporated in the PVA matrix to assess which were originated in the best results.

At first different amounts of CNC's (0.5, 1, 2 and 5 % m/m related to PVA mass) were incorporated in PVA 10 wt.% and the mixtures left to dry at room temperature overnight, until constant weight. By macroscopic evaluation (see Figure 4.11) it was possible to see white aggregates in concentrations as low as 1 wt.%, resulting in non-homogeneous samples.

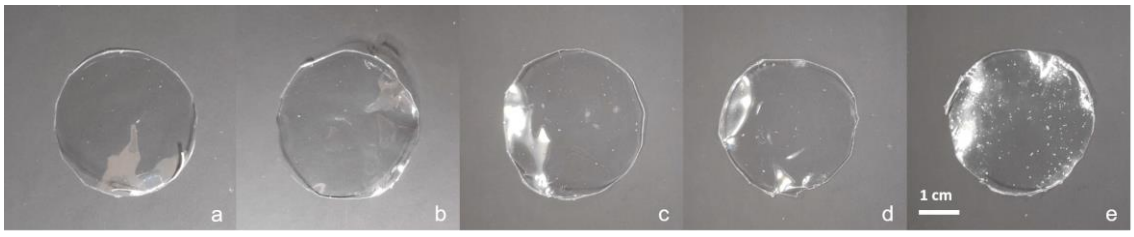

Figure 4.11 - Photographs of PVA films with increasing concentration of CNC: a) 0 wt.%, b) 0.5 wt.%, c) 1 wt.%, d) 2 wt.% e) 5 wt.%. Same scale applies to all of the images in the composition.

CNCs are meant to act as a mechanical reinforcement and Rescignano *et al*. already have showed that an increase in CNCs amount from 0.5 to 1 wt. % does not improve the mechanical properties of the final product, proving that the smaller amount results in the highest value for Young's modulus without compromising other mechanical properties [52]. Taking the literature and our own macroscopic observations, an amount of 0.5 % wt. of CNCs was selected.

The next goal was to identify the maximum load of SPIONs that could be incorporated in the composite system. Contents of 0.5 and 5 wt.% of SPIONs (in respect to the PVA content) were used in a mixture of 0.5 wt.% CNC/PVA and the solvent allowed to evaporate. Macroscopically, good incorporation and distribution of the SPIONs was verified along the films, so increasing concentrations of SPIONs were tested: 7.5 wt.% and 10 wt.% (see Figure 4.12 a). An incorporation of 10 wt.% SPIONs resulted in flexible and homogenous film, visible in Figure 4.12 b). Additionaly, the composite films incorporating SPIONs were able to respond to a permanent magnet.

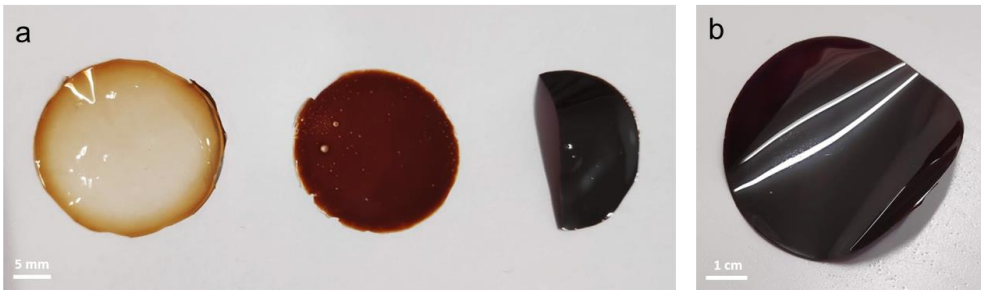

Figure 4.12 – a) Study of incorporation of SPIONs in PVA films obtained by solvent evaporation. From left to right: 0.5 wt.%, 5 wt.% and 7.5 wt.% SPIONs in respect to PVA content. b) CA-crosslinked film at 130 °C, with 10 wt.% SPIONs prior to washing.

4.3.1 Hybrid composite system crosslinking

PVA is a very hydrophilic material, readily soluble in water. To make this material suitable for biomedical applications, i.e., insoluble in water-based solutions, it must be crosslinked. Several crosslinking processes can be used, and within chemical crosslinking various options are described in literature: dialdehydes, dicarboxylic and tricarboxylic acids, diisocyanates and boric acid [69]. On one hand there is citric acid which is a non-toxic compound, while glutaraldehyde is a widely used crosslinker, being two acceptable choices for crosslinking this hybrid composite system. Citric acid crosslinks the polymer via esterification between the carboxyl groups of the carboxylic acid and the hydroxyl groups present in the polymer; whereas glutaraldehyde-crosslinking depends on the acetylation of hydroxyl (polymer) and aldehydic groups [39], [46]. It is well known that acidic environments can be advantageous since they catalyze the crosslinking reaction, so hydrochloric acid was used.

Taking these features into account, glutaraldehyde and citric acid were used to crosslink the developed hybrid composite system. Firstly, two concentrations of GA+HCl were tested, 10+4 % and 1+0.1 % m/m in respect to PVA content. This presented two extreme situations that resulted in the hydrogels presented in Figure 4.13: a) shows the hydrogel with the lowest concentration, no consistency is noticeable and it was not easily manageable; for the highest concentration (panel b), as soon as the catalyst came into contact with PVA the crosslinking reaction took place, entrapping the magnetic stirrer within

the structure. An intermediate concentration (5 % wt.) was set and the same amount was chosen for citric acid for practicality reasons. When concerning the catalyst, 2 % of HCl was chosen. When crosslinking with GA in the absence of HCl, films were obtained but these were readily soluble in water.

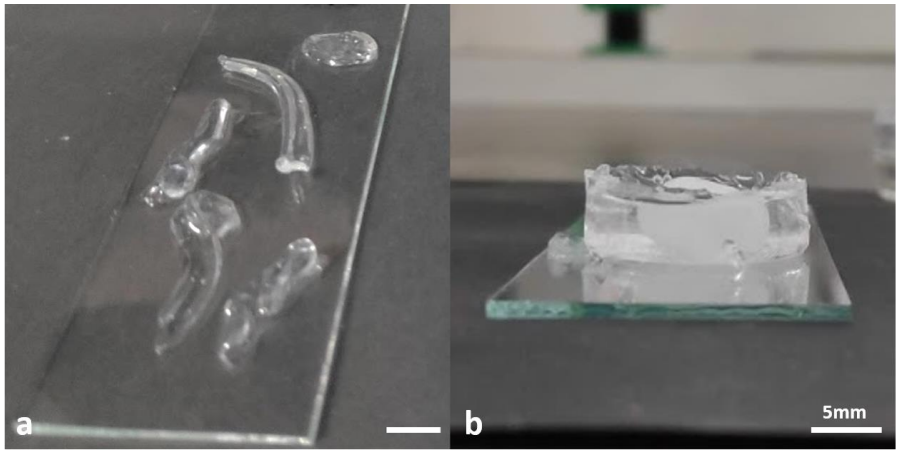

Figure 4.13 - Pre-study of the concentrations of crosslinker to be used. In the left picture a), 1 % of GA+ 0.4 % of HCl. In the right picture b), 10 % of GA + 4 % HCl.

For each crosslinker, the presence of catalyst and temperature were tested. In both cases, hydrochloric acid was used as catalyst, and its efficacy was tested by comparing the crosslinking efficiency with and without the presence of the catalyst. The several attempts and description of the obtained products are summarized in Table 4.2.

Table 4.2 –Tested conditions to crosslink the hybrid composite system depending on the crosslinking agent, presence of catalyst, reaction temperature, and the respective results.

Crosslinker	Catalyst	Crosslinking Temperature Reaction	Result
Citric acid		25-37 °C	Films soluble in water, SPIONs release
	HCl		Films soluble in water, SPIONs release
		90 ºC	Slight yellowing, lower swelling degree films
	HCl		Some browning, lower swelling degree films
		130 °C	Good swelling behavior films, yellowing
	HCl		Good swelling behavior films but severe darkening (Figure 4.14)
Glutaraldehyde		25 °C	Soluble in water films
	HCl		Hydrogel (Figure 4.16)

Citric acid did not effectively crosslink the samples at low temperatures (25 and 37 °C), even when the catalyst was added: the produced films were soluble in water, and the films that contained SPIONs turned the water a brown color, revealing a release of SPIONs from the structure. Some studies indicated that carboxylic acid crosslinking could only be achieved with temperatures as low as 90 °C, so that was the next approach[41]. This temperature affected the appearance of the films, presenting slight yellowing, and in the cases where catalyst was present, some browning. Although this temperature did

result in a better behavior in water, the films still swelled considerably. It is important to refer that various curing times were tried, not having resulted in relevant differences. The last tested temperature for citric acid films was 130 °C which produced films with satisfactory behavior while in contact with water. In the absence of catalyst, the films presented yellowing whereas catalyst-containing-films were severely darkened (Figure 4.14). This yellow appearance was expected and is reported in the literature [14]. The striking appearance of the catalyzed films at 130 °C indicated that some degradation could be happening. Taking this into account and considering that without catalyst the obtained films did not dissolve in water, it was chosen not to continue using HCl as catalyst in CA-crosslinked films. The minimal reaction time, at this temperature, necessary to verify crosslinking was also assessed and several tests were made revealing that 5 h in the oven presented the best macroscopical results, that originated a contact-lens kind of texture when hydrated (Figure 4.15).

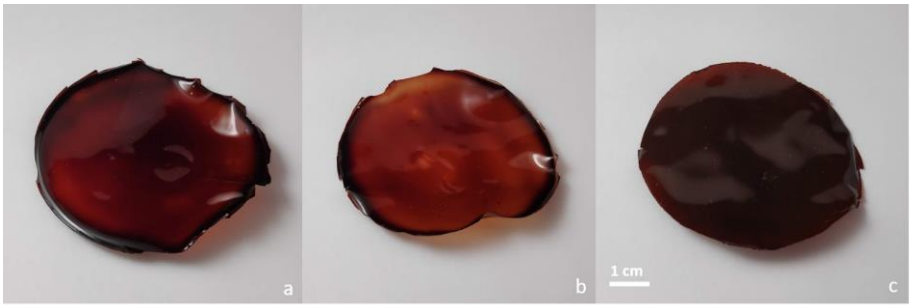

Figure 4.14 – Photographs depicting the obvious darkening of the citric acid-crosslinked films catalyzed with HCl at 130 °C. Top view of: a) PVA/CA b) PVA/CNC/CA and c) PVA/CNC/NP/CA. Same scale applies to all of the images in the composition.

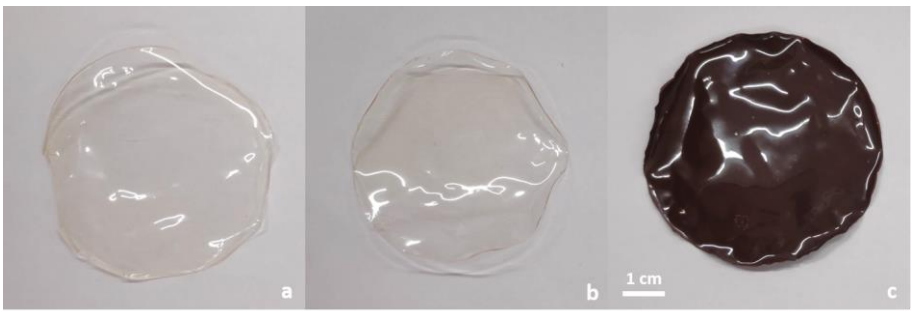

Figure 4.15 – Photographs of the top view of the optimized CA-crosslinked films at 130 ºC during 5 h in the absence of catalyst (after washing and drying): a) PVA, b) PVA/CNC and PVA/CNC/NP. Same scale applies to all of the images in the composition.

In the case of glutaraldehyde crosslinked hydrogels, the reaction occurred at room temperature, resulting in hydrogels which are able to swell but did not dissolve in water. Therefore, two different types of structures were obtained: citric acid crosslinked films cured at 130 °C (without catalyst) (Figure 4.15); glutaraldehyde crosslinked hydrogels catalyzed with HCl (Figure 4.16). Although the observation of good results with the latter crosslinking method, this procedure still had to be optimized, since upon addition of GA/HCl, aggregates were immediately formed in PVA, even with heavy magnetic stirring. To slow down the crosslinking reaction, the adding process was done with cold reagents, bypassing the aggregate formation. It is well known, that biological cells are very sensitive to acidic environments, and

since these composites both include an acid source, either citric or hydrochloric, any acidic residues needed to be removed by a washing process where the control of pH is done in order to attest the elimination of these products. The phosphate buffer solution and water used in the washing process of these samples were pH-measured to ensure no acidity in the samples. In this step, a slight yellow tinge in the liquid used to wash the films was noticed, which may indicate still some degree of release of nanoparticles. This wasn't observed in the washing of the GA-crosslinked samples. When dried, the hydrogel that contained SPIONs, presented the same behavior as the films in the presence of a permanent magnet.

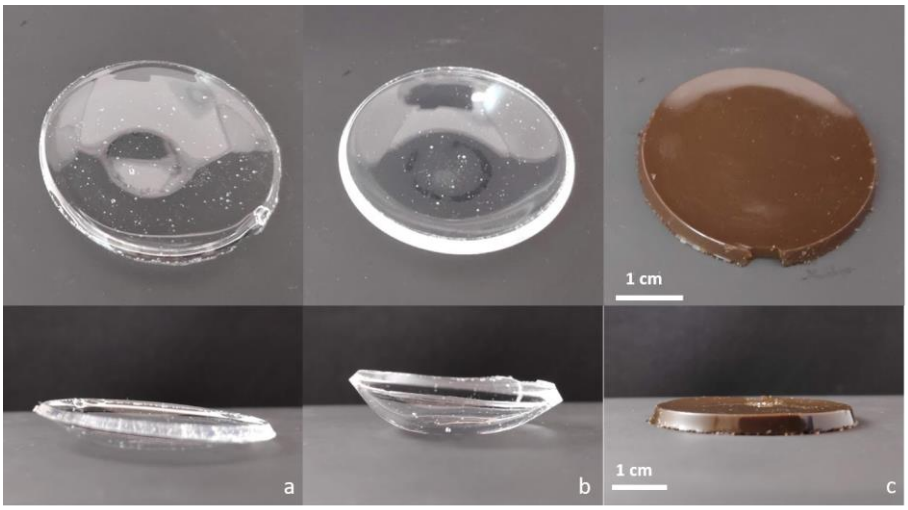

Figure 4.16 – Photographs of top and side view of the optimized GA-crosslinked hydrogels at room temperature: a) PVA b) PVA/CNC c) PVA/CNC/NP.

4.4 Hybrid composite system characterization

After optimization of the crosslinking procedure, both CA-films and GA-hydrogels were characterized. Firstly, XRD was used to structurally and chemically analyze and compare the produced composites. Observing Figure 4.17, pure PVA's characteristic peak is visible at 19.2° and a less visible characteristic peak of PVA is found at 40 °. It is also noticeable the right shift of the first peak in crosslinked samples in respect to neat PVA, which can indicate the crosslinking process in the crystalline domain, thus resulting in a compression of the amorphous region, making a more compact structure [70], [71]. The crystallinity in PVA and PVA CNC samples is attributed to PVA, while in the last sample, it is due to both PVA's polymer chains and Fe_3O_4 nanoparticles. DMSA-coated SPIONs characteristic (220) and (311) peaks are visible at 30° and 35° respectively. The rest of its characteristic peaks, (400), (511), and (440), usually present at 46, 57 and 63 ° may not be as visible due to their relative low amount in the sample. None of the characteristic cellulose peaks are visible in the composite samples, probably due to their very low amount in the mixture.

Figure 4.17 b) represents the obtained diffractograms from neat PVA and GA-crosslinked samples which include PVA, PVA/CNC and PVA/CNC/NP. The diffractograms of CA and GA-crosslinked samples have some similarities: both present the characteristic peak of PVA at 19.2 °, the characteristic DMSA-coated SPIONs peaks are visible and no CNCs characteristic peaks are noticeable. However,

there is no shift in the peaks like in the CA-crosslinked samples. Both diffractograms show that these samples are overall amorphous with no precise or narrow peaks, with the only crystallinity arising from the presence of PVA and SPIONs.

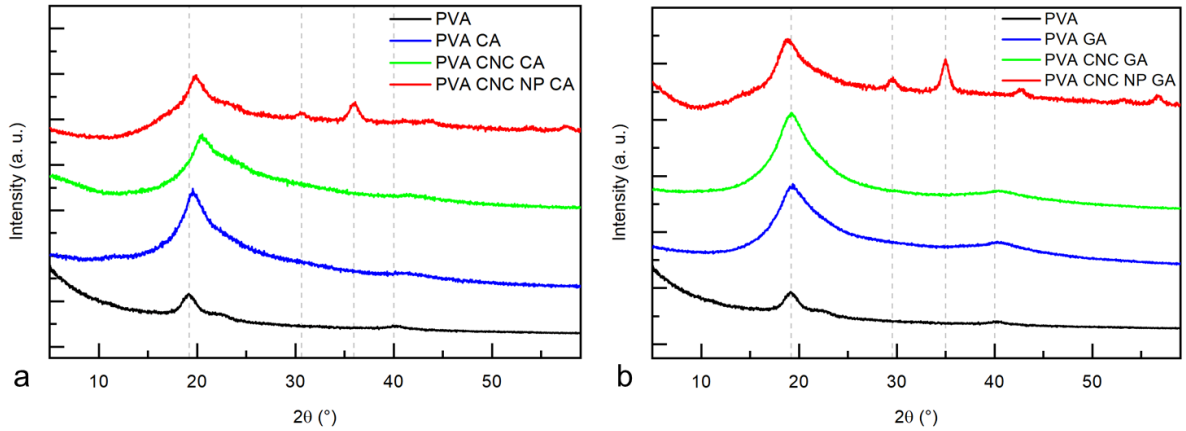

Figure 4.17 - XRD diffractograms for PVA, a) CA-crosslinked samples: PVA, PVA/CNC and PVA/CNC/NP, and b) GA-crosslinked samples: PVA, PVA/CNC and PVA/CNC/NP.

From Figure 4.18 a), if one looks at the FTIR spectrum of neat PVA, intramolecular and intermolecular hydrogen bonds are recognizable by the -OH vibration band between 3200 and 3360 cm^{-1}. Other characteristic bands of this material are due to alkyl groups, with C-H stretching between 2800 and 3000 cm^{-1}, and C-H bending at 1450 cm^{-1}. It's possible to identify the C=O linkage (1700-1725 cm^{-1}) attributed to non-hydrolyzed vinyl acetate, the precursor of polyvinyl alcohol. A slight increment is noticeable for all the CA-crosslinked samples in the carbonyl region (1715-1740 cm^{-1}) which indicates the presence of citric acid (lower wavenumber) and the ester (higher in the spectra) formed between PVA and CA. This increase is not associated with the presence of free citric acid, since the characteristic bands of carbonyls of carboxylic groups from citric acid are located at 1640, 1700 and 1790 cm^{-1} [46].

Concerning the samples crosslinked with glutaraldehyde and hydrochloric acid, FTIR analysis was also performed (Figure 4.18 b)). From these spectra, it is possible to notice an increase in the 2750 and 2850 cm^{-1} bands when comparing to neat PVA, correspondent to the C-H stretching of GA aliphatic chain. This band is stronger in the sample containing nanoparticles, possibly indicating a poorer crosslinking process. The carbonyl band (1720-1740 cm^{-1}) is stronger in PVA/GA and PVA/CNC/GA which may indicate a better crosslinking in these samples. These two bands in the 1500-1750 cm^{-1} region signal the GA-crosslinking of PVA, and although minor, they are visible. In the event of formation of acetal bridges, these should be noticeable in the 3200-3500 cm^{-1} region, although they aren't visible [39]. For both types of crosslinked samples, the reduced amount of crosslinker when compared with the amount of matrix may not be enough to manifest the typical decrease in -OH band intensity, which may also be masked by retained water in the composite.

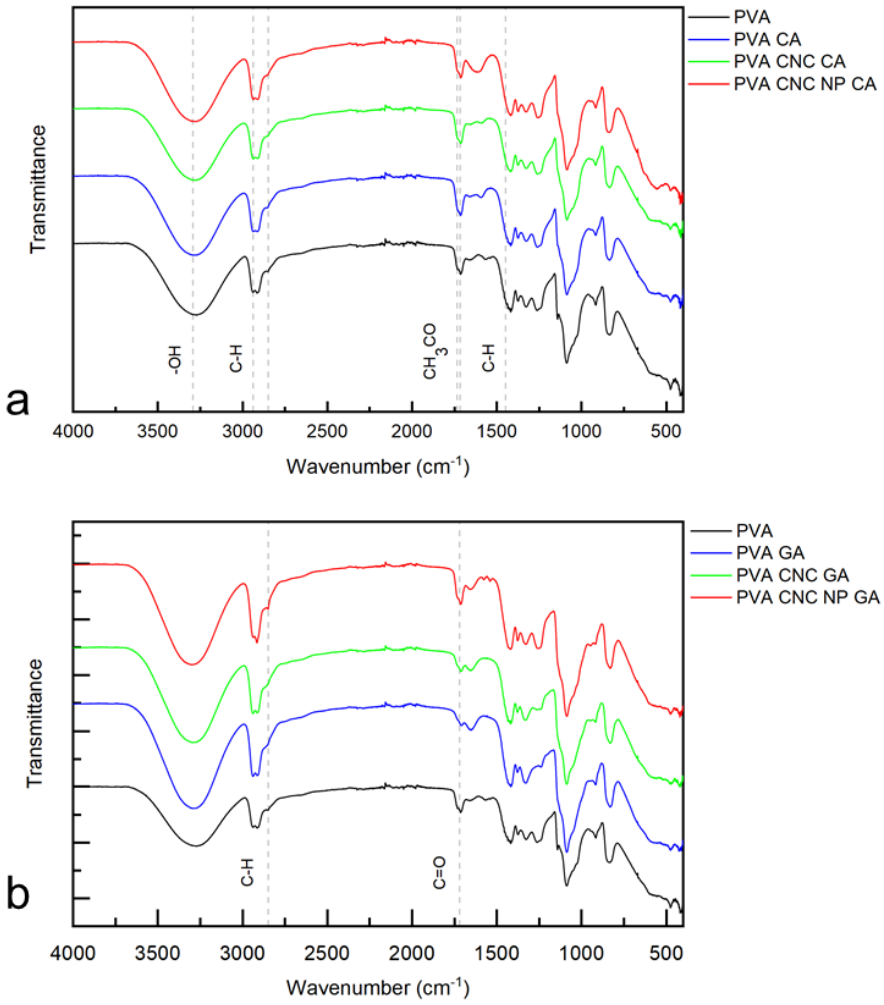

Figure 4.18 - FTIR spectra of a) citric acid-crosslinked PVA films and b) GA-crosslinked films: pristine PVA, crosslinked PVA film, PVA/CNC crosslinked films, and PVA/CNC/NP crosslinked films.

Analyzing Figure 4.19 a), PVA experiences a two-step degradation with a slight mass loss of 6.75% until 200 °C which can be attributed to loss of moisture [15]. The greatest weight loss in the polymer (71.96 %) is characteristic and noticeable between 200 and 400 °C, ascribed to the elimination of hydroxyl groups in the form of water and formation of polyene macromolecules [72]. CA-crosslinked PVA displays a very similar behavior, not showing any relevant differences when comparing with neat PVA which may be justified by the low amount of crosslinker. It would be expected of CNCs to grant better thermal stability to this composite given their *onset* temperature of 200 °C, but this is the only sample that has this different initial behavior, starting the degradation around 160 °C. Nevertheless, the amount of CNC is too low, and may not influence the composite in any way, being this unexpected behavior attributed to other phenomena. One possible explanation is that due to the presence of CNCs, this sample is more effectively crosslinked. In fact, this is the reported behavior of crosslinked PVA: citric acid crosslinked PVA is less thermally stable when comparing with neat PVA [15], [44], [45]. The sample containing SPIONS displays an abrupt loss of mass as do the other samples, although it is smaller (60 %). This loss in mass is stretched out across higher temperatures, which is attributable to the presence of nanoparticles, which are reportedly very thermally stable [73].

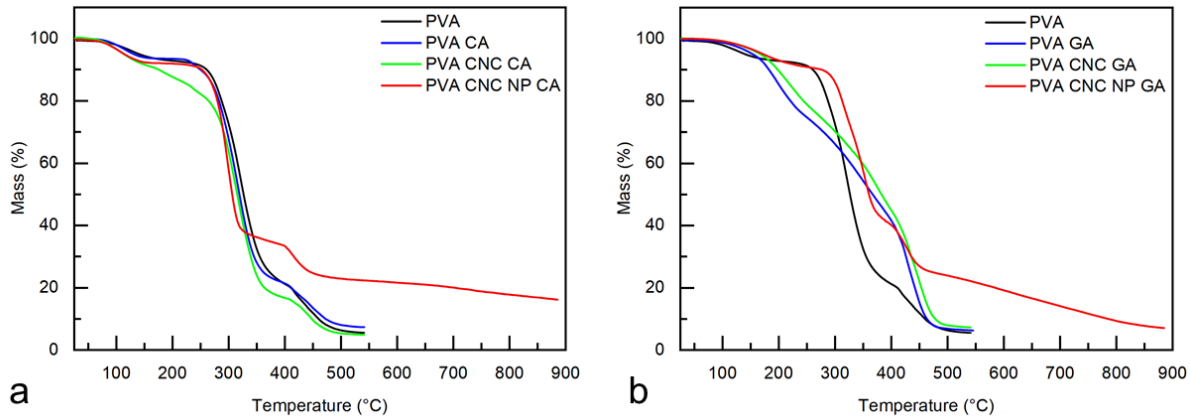

Figure 4.19 – Thermogravimetric analysis of neat PVA, a) CA-crosslinked and b) GA-crosslinked samples: PVA, PVA/CNC, PVA/CNC/NP.

GA-crosslinked PVA (Figure 4.19 b)) is not a two-step reaction: there is a gradual mass loss of about 20% until 200 °C and a more rapid decrease after it, until 480 °C. This behavior is also mimicked by PVA/CNC, with the latter only slightly shifted to the right. The low amount of CNC may be sufficient to notice a difference, but not enough to greatly affect the thermal endurance of the composite. The SPION-containing sample, is more peculiar, displaying a very similar performance to its CA-crosslinked counterpart. It is possible to conclude that ultimately, the incorporation of Fe_3O_4 nanoparticles grants better thermal endurance to both types of crosslinked samples.

It is known that CA-crosslinked PVA structures can swell up to 80 % of their initial weight [15]. Thus, this property was evaluated with water-uptake tests. The samples were put in water for a certain time, patted dry to remove excess water and weighed. They were then reintroduced in water for the chosen times and repetitively weighed. The weight swelling (S_w) ratio was calculated according to the following equation:

$$Sw\ (\%\ wt.) = \frac{(w_t - w_0)}{w_0} \times 100 \qquad \text{Equation 4.3}$$

Where w_t represents the weight at a given time and w_0 the initial weight. The swelling results were plotted as a function of time inside water (Figure 4.20)

When analyzing these results, it is possible to assert that all samples absorb at least their initial weight in water, without evolution after the 10 minutes time point. The error and wide variability in swelling weight may be due to human error, since the samples must be patted dry before weighing; or even due to environmental factors like the levels of humidity in the air which may affect the evaporation rate of water from the composite. One unexpected trend is the greater value for Sw (%) for PVA/CNC/CA: by having both PVA and CNC in the composite, it makes for a better crosslinking reaction, as seen before. The more crosslinked a polymer is, the less water the net is able to absorb. The sample containing nanoparticles displayed the greatest water uptake, since they seem less crosslinked than its counterpart samples.

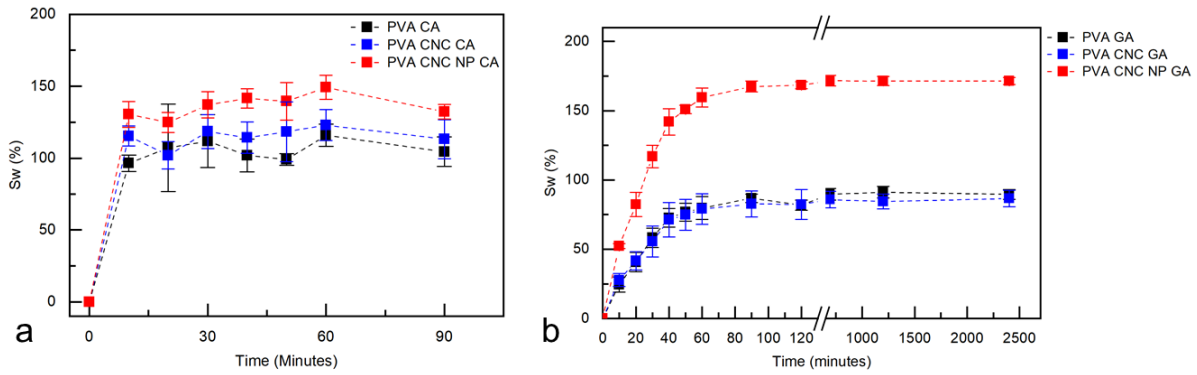

Figure 4.20 - Water uptake values for a) CA-crosslinked and b)GA-crosslinked PVA hydrogels: simple PVA/CA films, with CNC, and both CNC and SPIONs

For the water uptake assessment regarding GA-crosslinked samples, 90 minutes were not enough since the hydrogels only stabilized around 40 hours after the beginning of the test. Figure 4.20 b) presents two noticeably different trends: the nanoparticle-containing hydrogel absorbs 1.5 times its weight in water, double the capacity of its counterparts; neat PVA/GA and CNC containing samples absorb considerably less water, but PVA/CNC/GA takes up less water, indicating a more efficient crosslinking process. This is in accordance with the expected behavior: crosslinking presents double the efficiency because glutaraldehyde crosslinks both the PVA and CNCs.

There's a noticeable tendency in both CA and GA-crosslinked graphs: crosslinked PVA and crosslinked PVA with CNCs have very similar behaviors. From both materials it was possible to conclude that the presence of nanoparticles affects the efficacy of the crosslinking, granting a great swelling degree to these structures. One possible reason for this is that due to their size, DMSA-coated nanoparticles physically hinder the crosslinking reaction, impeding the ester linkages and acetal bridges from happening. This phenomenon was already reported in another polymer incorporating nanoparticles where the presence of nanoparticles disrupts the packing the chains, improving molecular transport [74]. This may help explain the behavior of the composites that feature SPIONs. In conclusion, none of these structures dissolved or disintegrate, and this high amount of nanoparticles doesn't prejudice the composite, if anything, it improves their water uptake.

Mechanical tests are important to assess the material's performance. For biomedical applications, and in this case specifically, in physiological environment it is important to guarantee the endurance of the biomaterials. What was noticeable when handling the previous material's samples for cell adhesion tests, was their brittleness and fragility. Although mechanical tests weren't performed in the previous material and comparisons can't be made, improvements were already visible and noticeable when handling the new samples. However, it is important to quantify those characteristics and compare them with the available literature. For films and membranes, tensile tests are the standard (since they didn't swell significantly in height) while for hydrogels usually compression tests are performed. In Figure 4.21 curves obtained from the tensile tests of neat PVA, and CA-crosslinked films in its different compositions, are pictured. On the right panel, an example of the test's apparatus.

Tensile tests were attempted for the CA-crosslinked films with a 100 N load cell and 2 mm/min speed until 95 N were reached. The CA-crosslinked PVA sample presents the typical behavior of PVA, reaching the plastic regime relatively fast, which reflects its plastic nature with a very small elastic region. PVA and crosslinked PVA show lower yield strengths of 10 and 19 MPa, respectively. The increase in this value between neat PVA and CA-crosslinked PVA was expected and well reported in the literature [44]. The incorporation of reinforcement in the form of CNCs is obvious in the other samples, with the much higher yield and Young's modulus. PVA/CNC and PVA/CNC/NP have enhanced toughness, with a very steep elastic regime and relatively high yield strength values of 52 and 80 MPa, respectively. Strong interactions between filler and matrix are achieved when incorporating CNCs in the PVA matrix, resulting in a restriction in matrix motion [57]. PVA displayed a Young's modulus of 4.58 ± 0.04 MPa, which is a very low value and discrepant with the literature's indicated values. More replicas should undergo tensile testing in order to understand this inconsistency in values. PVA CA presented a Young's modulus of 8.24 ± 0.04 MPa which is within the literature's expected values [15]. The incorporation of CNC exhibited a 16 MPa increase in Young's modulus (24.61 ± 0.09 MPa), proving its efficiency as reinforcement. PVA CNC CA NP showed the highest value for Young's modulus (56.16 ± 0.24 MPa) which suggests that incorporating both CNCs and SPIONs result in strong interactions between filler and matrix, promoting once again rigidity [75].

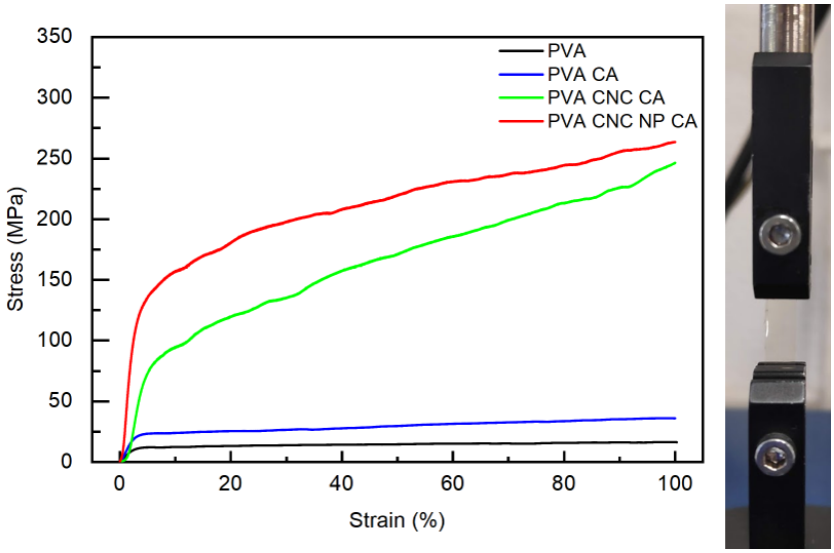

Figure 4.21 – On the left, tensile curves from neat PVA and CA-crosslinked films. PVA, PVA/CNC and PVA/CNC/NP all display typical behaviors. On the right, an example of the tensile test on the films.

Since the tensile tests are incomplete, i.e. weren't performed until break, some parameters like ultimate tensile strength and elongation at break are not determinable. Thus, some conclusions cannot be made, and results cannot be compared, although the trend of the curve implies that it is in accordance with literature. The reported ultimate tensile strength (UTS) for PVA is around 37 MPa, with an elongation at break of about 210 % [46], [69]. The values obtained for crosslinked PVA were very close to this, since the maximum stress value before the end of the test is 36 MPa in a region where the curve looks close to stabilizing. Values for strain also make sense, since in preliminary tests, it took two runs to break one sample, which is in accordance with the reported 210 % elongation. With the available load

cell and available displacement, fracture wasn't achieved. The dried films presented very little elastic regime, being only possible to inflict permanent deformation in the material. Another equipment is necessary to correctly study their mechanical behavior. A possible approach would be to test them in their hydrated state, as was done with the hydrogels, since they are decidedly more pliable and elastic, and this is the condition in which they would be hypothetically applied.

An example of a compression curve obtained from a compressive test with GA-crosslinked PVA hydrogel is pictured in Figure 4.22. All the curves obtained from the compression tests of the glutaraldehyde-crosslinked samples display the typical behavior of seen in hydrogels i.e. exponential curve. These were fitted through linear regression between 10 and 20 % strain, and the 3 best fittings were considered. All the data can be found in Supporting Information. The slope of these fittings was assumed as the compressive tangent modulus for 15 % strain. Values of 0.76 ± 0.22, 1.45 ± 0.55 and 1.05 ± 0.17 MPa were obtained for GA-crosslinked PVA, PVA/CNC and PVA/CNC/NP samples, respectively.

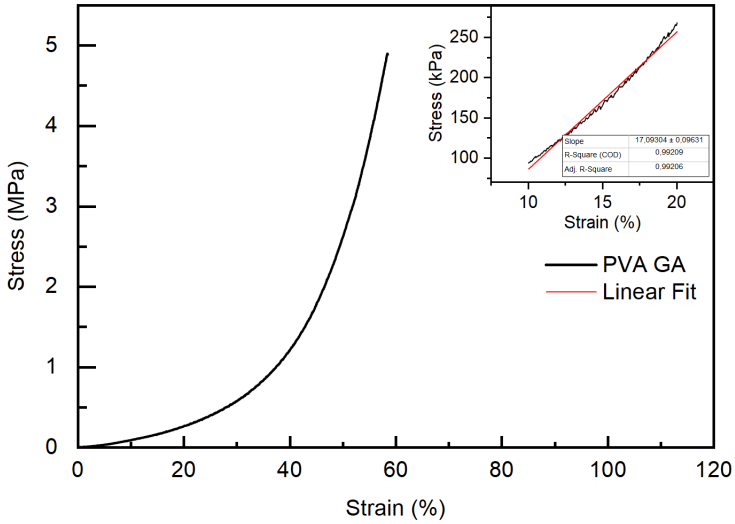

Figure 4.22 – Example of compression curve. In this graph of a GA-crosslinked PVA hydrogel, a steep exponential curve is observed until fracture. A close-up of the curve between 10 and 20 % deformation is pictured with its linear fit.

When looking at the obtained average values for each type of samples, the expected trend is noticeable. The first sample (PVA) displays the lowest compressive modulus since it does not incorporate the mechanical reinforcement. PVA/CNC displays a slightly higher value, concordant with the expected mechanical behavior for a reinforced composite. At last, PVA/CNC/NP displays an intermediate value: obviously better than the sample with no reinforcement, but not as good as the one with it, which also confirms the notion that NPs really do hinder proper crosslinking mechanisms. However, values are all within the errors of the other samples, not being enough to make certain conclusions. These are not easily comparable with literature, except for GA-crosslinked PVA, which presents acceptable values for the found references [76]. Additionally, it should be noted that PVA endured half of the tests, PVA/CNC only failed in three of ten runs. PVA/CNC/NP didn't reach 95 N of applied force in any of the tests, consistently failing in the range of 30-40 N of applied force or an average of 1.86 MPa.

Cytotoxicity assays show if a material is toxic to a cell line in its different concentrations. This is important because biomaterials for biomedical applications need to be biocompatible, and this is the first *in-vitro* checkpoint they must succeed in. While the previous material presented very satisfactory results, its poor handling properties led to a new formulation. Although only PVA was added, and this is known to be biocompatible, the concentrations of SPIONs and CNCs have shifted, and other crosslinkers and catalysts may affect their cytotoxic behavior. Cytotoxicity assays can be performed via three methods: extract, indirect and direct. In this case the extract method was used, in which the material to test is put in contact with culture medium. This culture medium is then diluted to several concentrations and put in contact in wells with seeded cells.

From Figure 4.23 it's possible to assert that PVA and PVA/CNC are not cytotoxic since they present very high values of cell viability, close to the negative control itself. However, the same cannot be concluded for the third material. The films that included nanoparticles, showed that the highest concentration (50 mg of material per mL of medium) is severely toxic. Nonetheless, the following concentrations are progressively less toxic, with the 25 mg/mL concentration achieving moderately cytotoxic values and the remaining two concentrations being classified as non-cytotoxic.

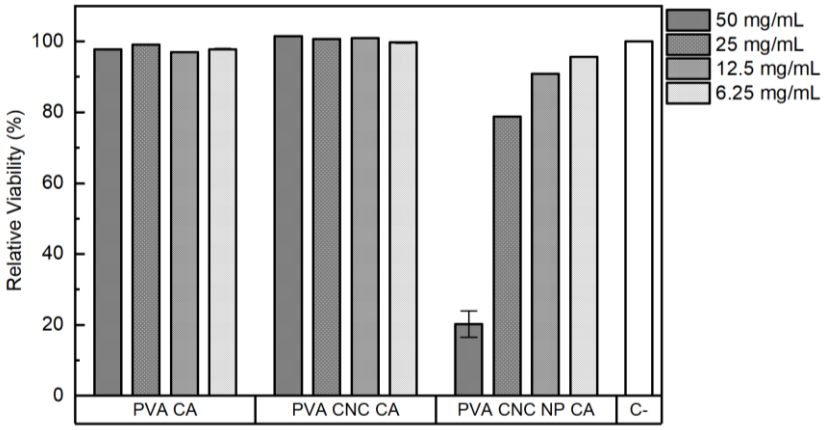

Figure 4.23 - Cytotoxicity of CA crosslinked films: PVA, PVA/CNC and PVA/CNC/NP were all tested for different concentrations (50, 25, 12.5 and 6.25 mg/mL). The last column, C-, refers to the values of the negative control.

The same trend can be confirmed in the cytotoxicity assays for the GA crosslinked composites (see Figure 4.24). Although the highest concentration for PVA/GA is bit more cytotoxic than the others, it's still within the acceptable error deviation. Both 50 and 25 mg/mL concentrations of PVA/CNC/NP remain cytotoxic in these samples. When looking at results from the two types of crosslinked samples, four situations are peculiar: CA-crosslinked PVA/CNC/NP in 50 and 25 mg/mL; and GA-crosslinked PVA/CNC/NP in 50 and 25 mg/mL. The elements in common between these are the presence of SPIONs and the higher concentrations, which indicates a possible cytotoxic effect that arises from their presence. Recalling the washing of the samples, a yellow tinge was noticeable, which could indicate release of the nanoparticles to the media. Some sources indicate 0.5 mg/mL of DMSA-coated SPIONs as the threshold for cytotoxicity [77]. In these samples, 10% of the composite is made up of Fe_3O_4 nanoparticles, which in 50 mg would amount to a theoretical mass of 5 mg of nanoparticles. If just 10%

of these are released, 500 µg are present in the media, which already presents cytotoxic effects in the cells.

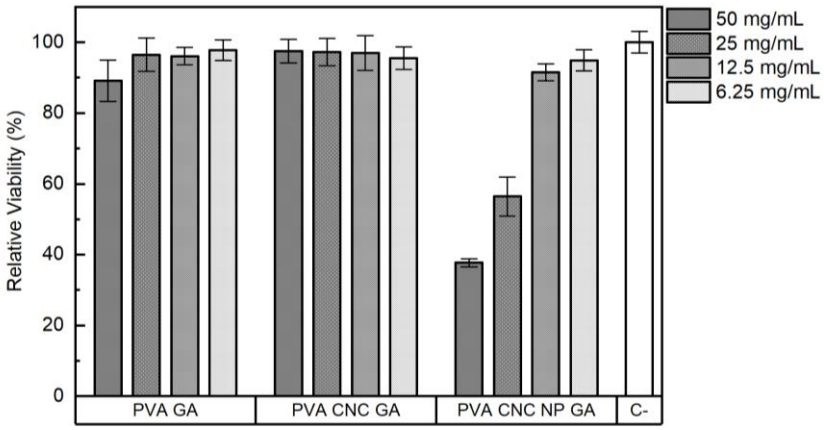

Figure 4.24 - Cytotoxicity of GA crosslinked gels: PVA, PVA/CNC and PVA/CNC/NP were all tested for different concentrations (50, 25, 12.5 and 6.25 mg/mL). The last column, C-, refers to the values of the negative control.

The materials' heating ability was tested with magnetic hyperthermia assays. Six 10 mg replicas of each sample were employed in this test, immersed in 1 mL of ultrapure water. Figure 4.25 represents the variation in temperature of each type of crosslinked sample that incorporates SPIONs. The highest temperature variation occurred for the glutaraldehyde hydrogel, and this can be explained by the relaxation mechanisms. In this type of material, SPIONs will have more degrees of freedom when compared to the films, justifying the difference in values. However, the relatively high deviation means these results are not conclusive, since the values of one sample are within the ranges of the other, and vice-versa. SPIONs dispersed in water presented higher variation in temperature, reaching between 3.5 and 4.9 °C which was expected, since Néel relaxation mechanism is predominant. Taking into account the body's normal temperature as 37 °C, for this amount of composite material and test parameters, it would reach 39.7 °C at most. Even though this value is far from the therapeutic temperature (42-43 °C), a longer test or more material could be attempted in order to achieve the necessary temperature.

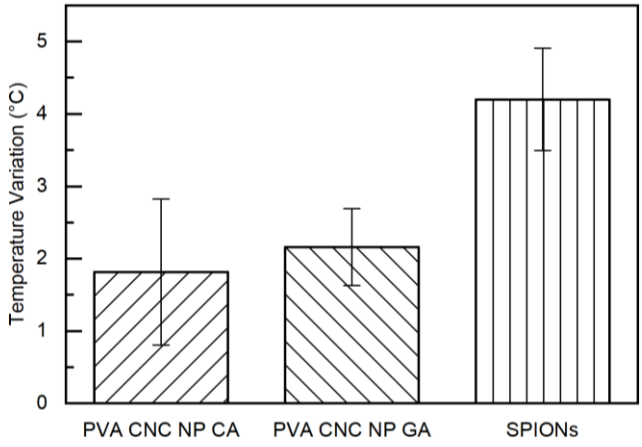

Figure 4.25 - Temperature variation depending on the type of sample: CA-crosslinked film or GA-crosslinked hydrogel. The same amount of SPIONs included in the samples was tested in solution for comparison sake.

5 Conclusions and Future Perspectives

The main goal of this work was the production of a CNC/SPIONs composite for magnetic hyperthermia application, that presented improved mechanical properties than the previously studied material. The previous study produced hybrid films of CNCs and SPIONs with iridescence (and therefore some degree of organization) not negatively affected by the presence Fe_3O_4. It produced a 1.5 °C increase in temperature under application of an AMF and although none of the materials tested positive for toxicity, adhesion and proliferation tests were still missing in order to have a full understanding of its interaction with cells.

Acid hydrolysis of microcrystalline cellulose was successfully employed, having been obtained cellulose nanocrystals. A 130 minutes reaction enabled the downsizing of 50 µm particles to nanorod-like particles with an average of 138 nm in length and width of 5 nm. The XRD diffractograms showed that, as expected, cellulose nanocrystals displayed a greater (92.10 %) crystallinity index than its precursor (88.24 %). This happens because the amorphous regions are cleaved off from the fiber, increasing the relative amount of crystalline domains. Its treatment was successfully executed with the aid of an ion-exchanging resin, and the substitution of H^+ by Na^+ was effectively confirmed by ICP. 4 wt.% CNC films were successfully produced with the obtained CNCs and used alongside the already produced hybrid composite, in cell adhesion and proliferation studies. Cells adhered satisfactorily and proliferation was well succeeded as well, although no orientation was observed. Still, the material was very difficult to handle, showing a brittle and fragile behavior. Thus, a new formulation was studied including PVA polymer, in order to grant malleability to the composite.

Superparamagnetic iron oxide nanoparticles were synthesized via chemical co-precipitation method and coated with dimercaptosuccinic acid to ensure stabilization and improved biocompatibility. Polyvinyl alcohol was a novelty in the composite when comparing with the previous material. Using the CNCs as reinforcement for this new composite, the three materials were combined and two types of structures were obtained, depending on the used crosslinker.

In XRD diffractograms, the typical PVA peak was noticeable in all the samples, although no characteristic CNC peaks were visible, probably due to the low amount present in the samples. In samples that contained SPIONS, the characteristic peaks were clearly visible, confirming their presence. TGA showed that all the samples containing SPIONs had a much higher thermal endurance, owing to the presence of magnetite itself. Water uptake tests exposed that films absorbed up to 1.5 times its weight in water. Hydrogels absorbed 0.75 times their weight in water, with the exception of PVA/CNC/NP which absorbed more than 1.5 times their weight in water. This may be indicative that nanoparticles hinder the effective crosslinking of the polymer chains leading to a greater water uptake. The fact that some nanoparticles may be released to the medium when the composite is hydrated can imply a good application for simultaneous magnetic hyperthermia and drug delivery.

In the continuation of this study, swelling tests at 37 °C may make sense to better simulate the body's atmosphere. Tensile tests with CA-crosslinked films showed that the presence of CNCs effectively strengthens the composite as well as the presence of SPIONs. It would be wise to repeat these tests

with the films in their hydrated state since it more effectively replicates their condition in physiological environment. The increase of almost 3 °C in magnetic hyperthermia is a promising result, although not sufficient to cause cell death. To further augment this temperature, other conditions may be tested such as increase the exposition time to the alternating magnetic field, tuning the magnetic field or higher amounts of material. While higher amounts of material would probably result in some cytotoxicity to the cells, a certain level of toxicity is tolerable when speaking of oncological therapies. The assessment of adhesion and proliferation of cells on these materials would be beneficial in order to predict its acceptance and biocompatibility by the body. In an aim to induce organization in the composite, another possible path may be tuning the relative amounts of CNCs, SPIONs and PVA, and study its influence in cell preferential adhesion and proliferation, since this is a more studied subject in tissue engineering. After extensive studies and improvements of its properties, this films/hydrogels could be hypothetically applied in an affected tumorous region after surgery, stopping further cancer development with preventive therapy.

6 References

[1] INE, DGS/MS, and PORDATA, “PORDATA - Óbitos de residentes em Portugal por algumas causas de morte,” 2019. [Online]. Available: https://www.pordata.pt/Portugal/Óbitos+de+residentes+em+Portugal+por+algumas+causas+de+morte-156. [Accessed: 06-Aug-2019].

[2] Eurostat, OMS, and PORDATA, “PORDATA - Óbitos: por algumas causas de morte,” 2019. [Online]. Available: https://www.pordata.pt/Europa/Óbitos+por+algumas+causas+de+morte-1612. [Accessed: 06-Aug-2019].

[3] SEER, “Cancer Statistics Review, 1975-2015 - SEER Statistics,” 2018. [Online]. Available: https://seer.cancer.gov/archive/csr/1975_2015/. [Accessed: 06-Aug-2019].

[4] P. I. P. Soares, I. M. M. Ferreira, R. A. G. B. N. Igreja, C. M. M. Novo, and J. P. M. R. Borges, “Application of hyperthermia for cancer treatment: recent patents review.,” *Recent Pat. Anticancer. Drug Discov.*, vol. 7, no. 1, pp. 64–73, Jan. 2012.

[5] R. Oun, Y. E. Moussa, and N. J. Wheate, “The side effects of platinum-based chemotherapy drugs: a review for chemists,” *Dalt. Trans.*, vol. 47, no. 19, pp. 6645–6653, May 2018.

[6] R. K. Gilchrist, R. Medal, W. D. Shorey, R. C. Hanselman, J. C. Parrott, and C. B. Taylor, “Selective Inductive Heating of Lymph Nodes,” *Ann. Surg.*, vol. 146, no. 4, p. 596, 1957.

[7] C. Sun, J. S. H. Lee, and M. Zhang, “Magnetic nanoparticles in MR imaging and drug delivery,” *Adv. Drug Deliv. Rev.*, vol. 60, no. 11, pp. 1252–1265, 2008.

[8] R. J. R. Matos, C. I. P. Chaparro, J. C. Silva, M. A. Valente, J. P. Borges, and P. I. P. Soares, “Electrospun composite cellulose acetate/iron oxide nanoparticles non-woven membranes for magnetic hyperthermia applications,” *Carbohydr. Polym.*, vol. 198, no. April, pp. 9–16, Oct. 2018.

[9] Z. K. Sadaf Afrin, “Nanocellulose as Novel Supportive Functional Material for Growth and Development of Cells,” *Cell Dev. Biol.*, vol. 04, no. 02, 2015.

[10] J. M. Dugan, J. E. Gough, and S. J. Eichhorn, “Directing the morphology and differentiation of skeletal muscle cells using oriented cellulose nanowhiskers,” *Biomacromolecules*, vol. 11, no. 9, pp. 2498–2504, 2010.

[11] J. M. Dugan, R. F. Collins, J. E. Gough, and S. J. Eichhorn, “Oriented surfaces of adsorbed cellulose nanowhiskers promote skeletal muscle myogenesis,” *Acta Biomater.*, vol. 9, no. 1, pp. 4707–4715, 2013.

[12] N. Lin and A. Dufresne, “Nanocellulose in biomedicine: Current status and future prospect,” *Eur. Polym. J.*, vol. 59, pp. 302–325, 2014.

[13] R. G. G. Martins, “Master Thesis Dissertation: Desenvolvimento de compósitos híbridos à base de nanocelulose e nanopartículas magnéticas para aplicações biomédicas,” Universidade Nova de Lisboa, 2018.

[14] C. Birck, S. Degoutin, N. Tabary, V. Miri, and M. Bacquet, “New crosslinked cast films based on poly(vinyl alcohol): Preparation and physico-chemical properties,” *Express Polym. Lett.*, vol. 8, no. 12, pp. 941–952, 2014.

[15] L. V. Thomas, U. Arun, S. Remya, and P. D. Nair, “A biodegradable and biocompatible PVA-citric acid polyester with potential applications as matrix for vascular tissue engineering,” *J. Mater. Sci. Mater. Med.*, vol. 20, no. SUPPL. 1, pp. 259–269, Dec. 2009.

[16] S. A. Paralikar, J. Simonsen, and J. Lombardi, “Poly(vinyl alcohol)/cellulose nanocrystal barrier membranes,” *J. Memb. Sci.*, vol. 320, no. 1–2, pp. 248–258, Jul. 2008.

[17] P. K. Deb, H. M. A. Odetallah, B. Al-Jaidi, R. R. Akkinepalli, A. Al-Aboudi, and R. K. Tekade, “Biomaterials and Nanoparticles for Hyperthermia Therapy,” in *Biomaterials and Bionanotechnology*, Academic Press, 2019, pp. 375–413.

[18] C. Blanco-Andujar *et al.*, “Design of iron oxide-based nanoparticles for MRI and magnetic hyperthermia,” *Nanomedicine*, vol. 11, no. 14. pp. 1889–1910, 2016.

[19] N. Lee, D. Yoo, D. Ling, M. H. Cho, T. Hyeon, and J. Cheon, “Iron Oxide Based Nanoparticles for Multimodal Imaging and Magnetoresponsive Therapy,” *Chem. Rev.*, vol. 115, no. 19, pp. 10637–10689, 2015.

[20] M. Häring, J. Schiller, J. Mayr, S. Grijalvo, R. Eritja, and D. D. Díaz, “Magnetic Gel Composites for Hyperthermia Cancer Therapy,” *Gels*, vol. 1, no. 2, pp. 135–161, 2015.

[21] B. Sanz, M. P. Calatayud, T. E. Torres, M. L. Fanarraga, M. R. Ibarra, and G. F. Goya, “Magnetic hyperthermia enhances cell toxicity with respect to exogenous heating,” *Biomaterials*, vol. 114, pp. 62–70, Jan. 2017.

[22] F. Wang *et al.*, “Injectable and thermally contractible hydroxypropyl methyl cellulose/Fe3O4 for magnetic hyperthermia ablation of tumors,” *Biomaterials*, vol. 128, pp. 84–93, 2017.

[23] E. A. Périgo *et al.*, “Fundamentals and advances in magnetic hyperthermia,” *Appl. Phys. Rev.*, vol. 2, no. 4, p. 041302, Dec. 2015.

[24] L. Kafrouni and O. Savadogo, “Recent progress on magnetic nanoparticles for magnetic hyperthermia,” *Prog. Biomater.*, vol. 5, no. 3–4, pp. 147–160, Dec. 2016.

[25] M. Mahmoudi *et al.*, “Optimal design and characterization of superparamagnetic iron oxide nanoparticles coated with polyvinyl alcohol for targeted delivery and imaging,” *J. Phys. Chem. B*, vol. 112, no. 46, pp. 14470–14481, 2008.

[26] M. Mahmoudi, H. Hofmann, B. Rothen-Rutishauser, and A. Petri-Fink, “Assessing the in vitro and in vivo toxicity of superparamagnetic iron oxide nanoparticles,” *Chem. Rev.*, vol. 112, no. 4, pp. 2323–2338, 2012.

[27] K. Hola, Z. Markova, G. Zoppellaro, J. Tucek, and R. Zboril, “Tailored functionalization of iron oxide nanoparticles for MRI, drug delivery, magnetic separation and immobilization of biosubstances,” *Biotechnol. Adv.*, vol. 33, no. 6, pp. 1162–1176, Nov. 2015.

[28] M. Auffan *et al.*, “In vitro interactions between DMSA-coated maghemite nanoparticles and human fibroblasts: A physicochemical and cyto-genotoxical study,” *Environ. Sci. Technol.*, vol. 40, no. 14, pp. 4367–4373, 2006.

[29] W. Y. Hamad, “Cellulose Nanocrystals: Properties, Production and Applications,” in *Cellulose Nanocrystals*, Chichester, UK: John Wiley & Sons, Ltd, 2017, p. 312.

[30] Z. Hosseinidoust, M. N. Alam, G. Sim, N. Tufenkji, and T. G. M. Van De Ven, “Cellulose nanocrystals with tunable surface charge for nanomedicine,” *Nanoscale*, vol. 7, no. 40, pp. 16647–16657, 2015.

[31] O. V Surov, M. I. Voronova, and A. G. Zakharov, “Functional materials based on nanocrystalline cellulose,” *Russ. Chem. Rev.*, vol. 86, no. 10, pp. 907–933, 2017.

[32] A. B. Reising, R. J. Moon, and J. P. Youngblood, “Effect of particle alignment on mechanical properties of neat cellulose nanocrystal films,” *J-for*, vol. 2, no. 6, pp. 32–41, 2012.

[33] B. L. Peng, N. Dhar, H. L. Liu, and K. C. Tam, “Chemistry and applications of nanocrystalline cellulose and its derivatives: A nanotechnology perspective,” *Can. J. Chem. Eng.*, vol. 89, no. 5, pp. 1191–1206, 2011.

[34] J. F. Revol, H. Bradford, J. Giasson, R. H. Marchessault, and D. G. Gray, “Helicoidal self-ordering of cellulose microfibrils in aqueous suspension,” *Int. J. Biol. Macromol.*, vol. 14, no. 3, pp. 170–172, Jun. 1992.

[35] R. M. Parker *et al.*, “The Self-Assembly of Cellulose Nanocrystals: Hierarchical Design of Visual Appearance,” *Adv. Mater.*, vol. 30, no. 19, pp. 1–13, 2018.

[36] A. B. Seabra, J. S. Bernardes, W. J. Fávaro, and A. J. Paula, “Cellulose nanocrystals as carriers in medicine and their toxicities : A review,” *Carbohydr. Polym.*, vol. 181, no. December 2017, pp. 514–527, 2018.

[37] M. Rajinipriya, M. Nagalakshmaiah, M. Robert, and S. Elkoun, “Importance of Agricultural and Industrial Waste in the Field of Nanocellulose and Recent Industrial Developments of Wood Based Nanocellulose: A Review,” *ACS Sustain. Chem. Eng.*, vol. 6, no. 3, pp. 2807–2828, Mar. 2018.

[38] A. Amanda and S. K. Mallapragada, “Comparison of Protein Fouling on Heat-Treated Poly(vinyl alcohol), Poly(ether sulfone) and Regenerated Cellulose Membranes Using Diffuse Reflectance Infrared Fourier Transform Spectroscopy,” *Biotechnol. Prog.*, vol. 17, no. 5, pp. 917–923, Oct. 2001.

[39] H. S. Mansur, C. M. Sadahira, A. N. Souza, and A. A. P. Mansur, “FTIR spectroscopy characterization of poly (vinyl alcohol) hydrogel with different hydrolysis degree and chemically crosslinked with glutaraldehyde,” *Mater. Sci. Eng. C*, vol. 28, no. 4, pp. 539–548, 2008.

[40] M. Djennad, D. Benachour, H. Berger, and R. Schomäcker, “Poly(vinyl alcohol) Ultrafiltration Membranes: Synthesis, Characterization, the Use for Enzyme Immobilization,” *Eng. Life Sci.*,

vol. 3, no. 11, pp. 446–452, 2003.

[41] B. Bolto, T. Tran, M. Hoang, and Z. Xie, “Crosslinked poly(vinyl alcohol) membranes,” *Prog. Polym. Sci.*, vol. 34, no. 9, pp. 969–981, 2009.

[42] M. A. Shakir, M. Firdaus Yhaya, and M. I. Ahmad, “The Effect of Crosslinking Fibers with Polyvinyl Alcohol Using Citric Acid,” *Imp. J. Interdiscip. Res. (IJIR*, vol. 3, no. 4, pp. 758–764, 2017.

[43] V. Coma, I. Sebti, P. Pardon, F. H. Pichavant, and A. Deschamps, “Film properties from crosslinking of cellulosic derivatives with a polyfunctional carboxylic acid,” *Carbohydr. Polym.*, vol. 51, no. 3, pp. 265–271, Feb. 2002.

[44] R. Shi *et al.*, “The effect of citric acid on the structural properties and cytotoxicity of the polyvinyl alcohol/starch films when molding at high temperature,” *Carbohydr. Polym.*, vol. 74, no. 4, pp. 763–770, Nov. 2008.

[45] S. Wang, J. Ren, W. Li, R. Sun, and S. Liu, “Properties of polyvinyl alcohol/xylan composite films with citric acid,” *Carbohydr. Polym.*, vol. 103, pp. 94–99, Mar. 2014.

[46] A. K. Sonker, A. K. Teotia, A. Kumar, R. K. Nagarale, and V. Verma, “Development of Polyvinyl Alcohol Based High Strength Biocompatible Composite Films,” *Macromol. Chem. Phys.*, vol. 218, no. 15, pp. 1–13, Aug. 2017.

[47] K. Pal, A. T. Paulson, and D. Rousseau, “Biopolymers in Controlled-Release Delivery Systems,” *Handb. Biopolym. Biodegrad. Plast.*, pp. 329–363, Jan. 2013.

[48] U. Brasch and W. Burchard, “Preparation and solution properties of microhydrogels from poly(vinyl alcohol),” *Macromol. Chem. Phys.*, vol. 197, no. 1, pp. 223–235, Jan. 1996.

[49] L. L. Lao and R. V. Ramanujan, “Magnetic and hydrogel composite materials for hyperthermia applications,” *J. Mater. Sci. Mater. Med.*, vol. 15, no. 10, pp. 1061–1064, Oct. 2004.

[50] S. Tanpichai and K. Oksman, “Cross-linked nanocomposite hydrogels based on cellulose nanocrystals and PVA: Mechanical properties and creep recovery,” *Compos. Part A Appl. Sci. Manuf.*, vol. 88, pp. 226–233, Sep. 2016.

[51] W. Li, R. Guo, Y. Lan, Y. Zhang, W. Xue, and Y. Zhang, “Preparation and properties of cellulose nanocrystals reinforced collagen composite films,” pp. 1131–1139, 2013.

[52] N. Rescignano *et al.*, “PVA bio-nanocomposites : A new take-off using cellulose nanocrystals and PLGA nanoparticles,” *Carbohydr. Polym.*, vol. 99, pp. 47–58, 2014.

[53] H. Yoshitake, K. Sugimura, Y. Teramoto, and Y. Nishio, “Magnetic property of oriented films of cellulose nanocrystal/carrageenan composites containing iron oxide nanoparticles: Effect of anisotropic aggregation of the nanoparticles,” *Polymer (Guildf).*, vol. 99, pp. 147–156, 2016.

[54] D. Shen, J. Liu, L. Gan, N. Huang, and M. Long, “Green Synthesis of Fe3O4/Cellulose/Polyvinyl Alcohol Hybride Aerogel and Its Application for Dye Removal,” *J. Polym. Environ.*, vol. 26, no. 6, pp. 2234–2242, Jun. 2018.

[55] T. Nypelö, C. Rodriguez-Abreu, J. Rivas, M. D. Dickey, and O. J. Rojas, “Magneto-responsive hybrid materials based on cellulose nanocrystals,” *Cellulose*, vol. 21, no. 4, pp. 2557–2566, 2014.

[56] T. Zhong, G. S. Oporto, J. Jaczynski, and C. Jiang, “Nanofibrillated cellulose and copper nanoparticles embedded in polyvinyl alcohol films for antimicrobial applications,” *Biomed Res. Int.*, vol. 2015, p. 456834, Jun. 2015.

[57] X. Xu, Y. Q. Yang, Y. Y. Xing, J. F. Yang, and S. F. Wang, “Properties of novel polyvinyl alcohol/cellulose nanocrystals/silver nanoparticles blend membranes,” *Carbohydr. Polym.*, vol. 98, no. 2, pp. 1573–1577, Nov. 2013.

[58] S. N. Fernandes *et al.*, “Mind the Microgap in Iridescent Cellulose Nanocrystal Films.,” *Adv. Mater.*, vol. 29, no. 2, p. 1603560, 2017.

[59] P. I. P. Soares *et al.*, “Effects of surfactants on the magnetic properties of iron oxide colloids,” *J. Colloid Interface Sci.*, vol. 419, pp. 46–51, Apr. 2014.

[60] M. D. Xue, T. Kimura, J. F. Revol, and D. G. Gray, “Effects of ionic strength on the isotropic-chiral nematic phase transition of suspensions of cellulose crystallites,” *Langmuir*, vol. 12, no. 8, pp. 2076–2082, Apr. 1996.

[61] W. Y. Hamad and T. Q. Hu, “Structure-process-yield interrelations in nanocrystalline cellulose extraction,” *Can. J. Chem. Eng.*, vol. 88, no. 3, pp. 392–402, 2010.

[62] J.-L. Huang, C.-J. Li, and D. G. Gray, “Cellulose Nanocrystals Incorporating Fluorescent Methylcoumarin Groups,” *ACS Sustain. Chem. Eng.*, vol. 1, no. 9, pp. 1160–1164, Sep. 2013.

[63] D. Gaspar *et al.*, “Nanocrystalline cellulose applied simultaneously as the gate dielectric and the substrate in flexible field effect transistors,” *Nanotechnology*, vol. 25, no. 9, p. 094008, Mar. 2014.

[64] L. Segal, J. J. Creely, A. E. Martin, and C. M. Conrad, “An Empirical Method for Estimating the Degree of Crystallinity of Native Cellulose Using the X-Ray Diffractometer,” *Text. Res. J.*, vol. 29, no. 10, pp. 786–794, Oct. 1959.

[65] R. Sunasee, U. D. Hemraz, and K. Ckless, “Cellulose nanocrystals: a versatile nanoplatform for emerging biomedical applications,” *Expert Opinion on Drug Delivery*, vol. 13, no. 9. pp. 1243–1256, 2016.

[66] D.-Y. Kim, Y. Nishiyama, M. Wada, and S. Kuga, “High-yield Carbonization of Cellulose by Sulfuric Acid Impregnation,” *Cellulose*, vol. 8, no. 1, pp. 29–33, 2001.

[67] M.-C. Popescu, “Structure and sorption properties of CNC reinforced PVA films,” *Int. J. Biol. Macromol.*, vol. 101, pp. 783–790, Aug. 2017.

[68] G. K. Tummala, I. Bachi, and A. Mihranyan, “Role of solvent on structure, viscoelasticity, and mechanical compressibility in nanocellulose-reinforced poly(vinyl alcohol) hydrogels,” *J. Appl. Polym. Sci.*, vol. 136, no. 6, pp. 1–8, 2019.

[69] A. K. Sonker, K. Rathore, R. K. Nagarale, and V. Verma, “Crosslinking of Polyvinyl Alcohol (PVA)

and Effect of Crosslinker Shape (Aliphatic and Aromatic) Thereof," *J. Polym. Environ.*, vol. 26, no. 5, pp. 1782–1794, 2018.

[70] M. C. Burshe, S. B. Sawant, J. B. Joshi, and V. G. Pangarkar, "Sorption and permeation of binary water-alcohol systems through PVA membranes crosslinked with multifunctional crosslinking agents," *Sep. Purif. Technol.*, vol. 12, no. 2, pp. 145–156, Nov. 1997.

[71] M. Abdelaziz and E. M. Abdelrazek, "Effect of dopant mixture on structural, optical and electron spin resonance properties of polyvinyl alcohol," *Phys. B Condens. Matter*, vol. 390, no. 1–2, pp. 1–9, Mar. 2007.

[72] V. S. Ghorpade, R. J. Dias, K. K. Mali, and S. I. Mulla, "Citric acid crosslinked carboxymethylcellulose-polyvinyl alcohol hydrogel films for extended release of water soluble basic drugs," *J. Drug Deliv. Sci. Technol.*, vol. 52, pp. 421–430, Aug. 2019.

[73] B. R. Ong, N. K. Devaraj, M. Matsumoto, and M. H. Abdullah, "Thermal stability of magnetite (Fe3O4) nanoparticles," in *Materials Research Society Symposium Proceedings*, 2008, vol. 1118, pp. 56–62.

[74] T. C. Merkel *et al.*, "Sorption, transport, and structural evidence for enhanced free volume in poly(4-methyl-2-pentyne)/fumed silica nanocomposite membranes," *Chem. Mater.*, vol. 15, no. 1, pp. 109–123, 2003.

[75] S. Azizi, M. Bin Ahmad, M. Z. Hussein, N. A. Ibrahim, and F. Namvar, "Preparation and properties of poly(vinyl alcohol)/chitosan blend bionanocomposites reinforced with cellulose nanocrystals/ZnO-Ag multifunctional nanosized filler.," *Int. J. Nanomedicine*, vol. 9, pp. 1909–17, 2014.

[76] P. K. Watler, C. H. Cholakis, and M. V. Sefton, "Water content and compression modulus of some heparin-PVA hydrogels," *Biomaterials*, vol. 9, no. 2, pp. 150–154, 1988.

[77] M. B. de S. Baptista, "Desenvolvimento de novas nanopartículas magnéticas para teragnóstico," Faculdade de Ciências e Tecnologia da Universidade Nova de Lisboa, 2017.

[78] X. M. Dong and D. G. Gray, "Effect of Counterions on Ordered Phase Formation in Suspensions of Charged Rodlike Cellulose Crystallites," *Langmuir*, vol. 13, no. 8, pp. 2404–2409, Apr. 1997.

[79] M. Talelli *et al.*, "Superparamagnetic Iron Oxide Nanoparticles Encapsulated in Biodegradable Thermosensitive Polymeric Micelles: Toward a Targeted Nanomedicine Suitable for Image-Guided Drug Delivery," *Langmuir*, vol. 25, no. 4, pp. 2060–2067, Feb. 2009.

[80] N. Fauconnier, J. N. Pons, J. Roger, and A. Bee, "Thiolation of maghemite nanoparticles by dimercaptosuccinic acid," *J. Colloid Interface Sci.*, vol. 194, no. 2, pp. 427–433, Oct. 1997.

[81] H. Xie *et al.*, "Lactoferrin-conjugated superparamagnetic iron oxide nanoparticles as a specific MRI contrast agent for detection of brain glioma in vivo," *Biomaterials*, vol. 32, no. 2, pp. 495–502, Jan. 2011.

7 Supporting information

7.1 Cellulose Nanocrystals

For the cellulose nanocrystals's synthesis, the following reagents were used: microcrystalline cellulose Avicel® PH-101 with ~ aprox. 50 µm particle size and 95% sulphuric acid (H_2SO_4), both from Sigma-Aldrich. The used water was obtained through the purification system Elix® Advantage 3 by Merck Millipore. The production method followed was described elsewhere by S. N. Fernandes *et al*. [58]. Acid hydrolysis of 15 g of microcrystalline cellulose took place with sulphuric acid (64 wt%) following an acid/solid ratio of 8.5:1. The reaction was stopped after 2 h and 10 min at 45 °C and always under magnetic agitation (500 rpm). 10 times the suspension's volume of water were added in order to quench the reaction. Washing with Ultrapure water and removal of supernatant were followed until pH=0.7. The following washes were done alongside centrifugation cycles at 12000 rpm for 20 minutes (ThermoFisher Scientific, Heraeus Multifuge X1R). CNCs were collected when the pellet was visible and pH was close to 1.4 - 1.9. Dialysis was followed to further increase the pH value. This was done using a dialysis membrane with a 12-14 kDa cutoff against ultrapure water until the water's pH was constant (around 5,5 - 6), taking approximately a month. The CNC suspension was collected, and its concentration was calculated through the gravimetry method. This consists in putting 50 uL of suspension in eppendorfs and drying them in the oven at 60 °C, progressively weighing them until a constant weight was registered. The suspension presented a 1.14 %wt.

After PEG-dialysis aided concentration (described in section 3.1 of Materials and Methods), the 6 wt.% CNC-Na suspension was diluted to 4 wt.% and submitted to ultrasound for 20 minutes with a pulse of 0.8 and 85 % of the maximum power. Subsequently, 1 mL was deposited into each well of a 24 well plate. The plate was left in a 37 °C oven until complete solvent evaporation was observed (controlled by the lack of changes in the weight of the samples). Due to their easy dispersion in water, the films were stabilized through a thermal treatment at 35 ºC in vacuum for 24 h previously reported in the work of Dong and Gray [78].

7.2 Iron Oxide Nanoparticles' Synthesis

Hexa ($FeCl_3.6H_2O$) and tetrahydrate ($FeCl_2.4H_2O$) iron chlorides (Sigma Aldrich) were used in the Fe_3O_4 nanoparticle synthesis, as well as a 25% ammonia solution (NH_4OH, Panreac) and ultrapure water. For the iron content determination, a few reagents were used: hydrochloric acid 37% v/v (HCl, Carlo Erba), hydroxylamine (H_3NO, Alfa Aesar), phenanthroline ($C_{12}H_8N_2$, Applichem) and ammonia acetate ($C_2H_7NO_2$, Sigma Aldrich).

For the coating of the nanoparticles, nitric acid 65% v/v (HNO_3, Panreac), previously prepared hydrochloric acid 0.01 N (HCl, Carlo Erba) and sodium hydroxide 0,01 N (NaOH, Sigma Aldrich), and dimercaptosuccinic acid (DMSA, $C_4H_6O_4S_2$ by Sigma Aldrich).

The magnetic nanoparticles were synthesized by the chemical precipitation method, described elsewhere by P. I. Soares *et al*.[59]. Both the ferrous (2.5 mmol) and ferric (5 mmol) chlorides were dissolved

in 100 mL of ultrapure water. The solution was submitted to mechanical stirring (700 rpm) and to deaeration of O_2 by bubbling with N_2. 10 mL of the ammonia solution were rapidly added and left stirring for 5 minutes. After this time had passed, 60 mL of ultrapure water were added to quench the reaction. A strong magnet was put on the bottom of the beaker and the nanoparticles were left to precipitate. The supernatant was discarded, the nanoparticles were washed with ultrapure water and left to precipitate. This washing step was repeated two more times.

To determine the concentration of Fe_3O_4 nanoparticles - and subsequently the amount of surfactant to add - the colorimetric method of 1-10-phenanthroline was used [79]. A hydrochloric acid solution was prepared, subsequently used in the production of the hydroxylammonium chloride (100 $mg.mL^{-1}$), phenanthroline (3 $mg.mL^{-1}$) and ammonium acetate (500 mM) solutions. Next, a dilution of the nanoparticles solution was made in a 1:250 proportion, from which 40 µL were put into an Eppendorf. In this Eppendorf 20 µL of 37% v/v hydrochloric acid were added and left to react at room temperature for an hour. After this, 100 µL of hydroxylamine solution and 500 µL of phenanthroline solution were added, and this mixture was diluted to a final volume of 1800 µL with ammonium acetate. This was repeated for a total of 5 eppendorfs. The absorbance of the samples at 510 nm was measured using the spectrophotometer UV-VIS (T90+ UV/VIS Spectrometer PG Instruments Ltd.).

The sample's iron concentration was calculated with the calibration curve:

$$Abs=4,5079\times[Fe]+0,0753 \qquad \text{Equation 7.1}$$

In this equation Abs is the average of the obtained values for 510 nm and [Fe] the iron concentration present in the samples, given in mg/mL. This value is then multiplied by the dilution factor to obtain the real value. To determine the concentration of nanoparticles present in the sample, the following equation is used, obtained experimentally:

$$[Fe]=0,7\times[NPs] \qquad \text{Equation 7.2}$$

To increase the stability of the magnetite nanoparticles, a DMSA coating was applied following the works of Fauconnier and Xie *et al*. [80], [81]. For the coating process to be efficient, the pH value of the nanoparticle suspension must be between 3 and 3,5. This correction is done with the controlled addition of nitric or hydrochloric acid. The DMSA solution, already dissolved in ultrapure water with the final volume of 10 mL must have a pH of 5,5 adjusted in the same manner with the use of sodium hydroxide. The number of moles used in the DMSA solution must be calculated in function of the iron concentration in the nanoparticles suspension (3% of the number of moles of iron). Both the solutions are added and kept for three hours in a ultrasound bath.

7.3 In vitro tests

7.3.1 Cytotoxicity Assays Procedure

For these assays, 150 mg of each of the three types of CA crosslinked samples were weighed and put in an oven at 120 °C for 2 hours. About 1970 mg of each type of GA-crosslinked samples were weighed, put in an oven at 120 °C overnight, submerged in 70% ethanol and left to dry for a day in the

laminar flow chamber. To produce the extract 1.5 mL and 4 mL of culture medium (DMEM by Sigma-Aldrich) were added to each one of the samples crosslinked by citric acid and glutaraldehyde respectively and left at 37 °C for 2 days. Vero cells, epithelial cells extracted from the kidney of the African green monkey, had been previously seeded in DMEM with a cell density of approximately 6 kC/well. 5 replicas of each of the 4 dilutions for each material were made, as well as positive, negative and cell medium control wells. The positive control wells included 10 % of dimethyl sulfoxide (DMSO, Sigma-Aldrich), a substance that impedes cell viability. Resazurin is a blue non-fluorescent dye that can be used as a pH indicator but as a viability indicator as well. It shows very low cytotoxicity which makes it a good candidate when compared to other types of assays. This reagent is reduced to resorufin, a pink and fluorescent product when metabolized by active cells. This change in color is measured by absorbance and is proportional to the number of viable cells. The measurements are done at 601 and 571 nm, which are the absorbance peaks of resazurin and resorufin, respectively. The readings were made by the well plate reader *Biotek ELX 800 UV*.

7.3.2 Cell Adhesion and Proliferation Assays

Firstly, the samples were sterilized by submerging them in 70 % ethanol for 30 minutes, which was subsequently aspired and left to dry in the laminar flux chamber. The samples were then put on top of a glass coverslip and between the Teflon ring, with DMEM inside each well. Vero cells were seeded with a cell density of 40 kC/well on 5 replicas of each sample. The cells were incubated at 37 °C in a controlled 5 % CO_2 atmosphere for 24 h. To determine the adhesion and proliferation of cells, the Resazurin Reduction assay was performed. The medium was substituted by a 1:1 solution of resazurin and DMEM and left to incubate for 3 hours. This was done for every reading, followed by washing of the well and addition of new medium. Absorbance measurements were made after 1, 3, 6, 8.5 and 10 days. Staining was performed with DAPI and phalloidin after fixation.

7.4 Characterization Techniques

Fourier Transform Infrared (FTIR) spectroscopy was conducted with PerkinElmer Spectrum Two spectrometer in several samples (4 scans per sample), with the attenuated total reflectance (ATR) accessory at room temperature between 4000 and 400 cm^{-1}. X-Ray Diffraction (XRD) diffractograms were obtained using the PANanalytical X'Pert PRO equipment with Bragg-Brentano (θ/2θ coupled) geometry with graphite monochromated Cu KR (1.54 Å) radiation. A scanning step of 2θ=0.00334 ° collected data from 10 ° to 40 °. A heating rate of 5 °C/min was used from 25 to 550 °C (or 900 °C depending on the sample) when acquiring information from the Netzsch 449 F3 Jupiter® simultaneous thermal analyzer for thermogravimetric analysis measurements. The size and morphology of the CNCs were analyzed with atomic force microscopy (AFM) using an Asylum Research MFP-3D standalone system in tapping mode, with silicon AFM probes (scanning frequency of 300 kHz, k=26 N/m). To do this, 1 µL ultra-diluted suspension's droplets (0.01% w/w) were cast on a mica substrate. The obtained images were analyzed with the aid of Gwyddion software. Thicknesses were measured with a Mitutoyo digital micrometer. For ICP-AES analysis, 2.7 mg of CNC Na were digested in 500 µL of nitric acid p.a. for 1 hour or until full dissolution.

7.5 Mechanical Tests

Data obtained from the compression test runs is presented below. The highlighted rows present the highest R^2 adjustment, therefore used in the calculation of the compressive tangent modulus. Examples of the obtained graphs are presented as well.

Table 7.1 - Data obtained from the GA crosslinked PVA hydrogel for the compressive test runs

Sample	Slope	R^2	Average	Standard Deviation	
17	318136,5	0,99682	764966,6	219740,5	Pa
18	874931,1	0,99853	0,76	0,22	MPa
19	438243,8	0,99669			
20	1,71E+06	0,99206			
21	760322,2	0,99891			
22	1,59E+06	0,99289			
23	986992,5	0,99925			
24	607638,6	0,99751			
25	979634,2	0,99456			
26	1,07E+06	0,99774			
27	547585,2	0,99937			

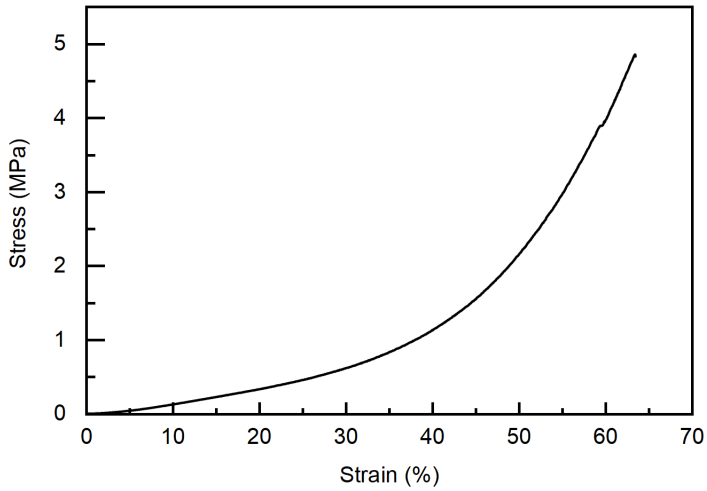

Figure 7.1 - Example of compression curve. In this graph of a GA-crosslinked PVA/CNC hydrogel, a steep exponential curve is observed until fracture.

Table 7.2 - Data obtained from the GA crosslinked PVA/CNC hydrogel for the compressive test runs

Sample	Slope	R^2	Average	Standard Deviation	
28	2,05E+06	0,99972	1,45E+06	551514,7	Pa
29	2,03E+06	0,99919	1,45 Mpa	0,55	Mpa
30	966515,2	0,99078			
31	1,31E+06	0,99924			
32	2,84E+06	0,99708			
33	1,76E+06	0,99718			
34	2,51E+06	0,99686			
35	3,42E+06	0,99018			
36	1,86E+06	0,99877			
37	1,47E+06	0,99856			
38	974400,3	0,99928			
39	3,98E+06	0,99269			
40	1,51E+06	0,99917			

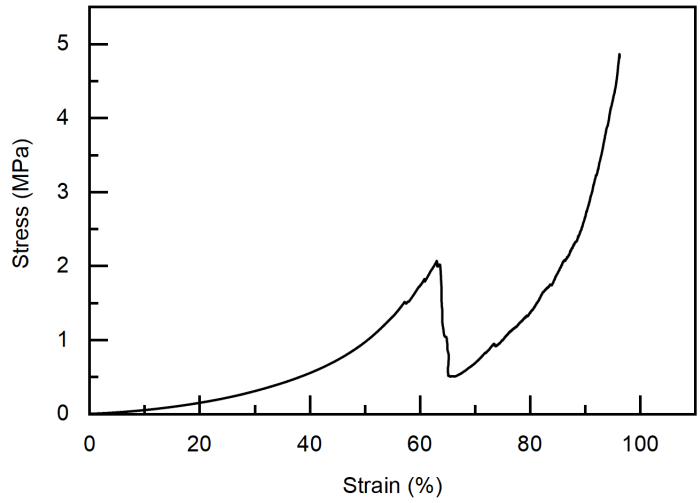

Figure 7.2 - Example of compression curve. In this graph of a GA-crosslinked PVA/CNC/NP hydrogel, a steep exponential curve is observed until fracture.

Table 7.3 - Data obtained from the GA crosslinked PVA/CNC/NP hydrogel for the compressive test runs

Sample	Slope	R^2	Average	Standard Deviation	
41	560788,7	0,98753	1,05E+06	168407,1	Pa
42	321613,9	0,96434	1,05	0,17	Mpa
43	1,24E+06	0,9994			
44	646718,2	0,9813			
45	930251,4	0,99768			
46	566345,3	0,9922			
47	983473,2	0,99582			
48	535754,6	0,98893			
49	972240,1	0,99738			
50	359675,3	0,97814			